Ōhiwa Harbour Delft3D sediment transport modelling to support the National Policy Statement on Freshwater (NPS-FM)

ERI REPORT NUMBER 162

by

Bryan, K.R, Stewart, B., Rahdarian, A. Rautenbach, C.

Client report prepared for

Bay of Plenty Regional Council

8 February, 2023

Email: Karin.bryan@waikato.ac.nz

Environmental Research Institute
Division of Health, Engineering, Computing & Science
University of Waikato, Private Bag 3105
Hamilton 3240, New Zealand

THE UNIVERSITY OF WAIKATO
Te Whare Wānanga o Waikato

Te Tumu Whakaora Taiao
Environmental Research Institute
THE UNIVERSITY OF WAIKATO

Cite report as:

Bryan KR, BT Stewart, A Rahdarian and C Rautenbach. 2023. Ōhiwa Harbour Delft3D sediment transport modelling to support the National Policy Statement on Freshwater (NPS-FM). *Environmental Research Institute Report No. 162*. Client report prepared for Bay of Plenty Regional Council. Environmental Research Institute, Division of Health, Engineering, Computing & Science, The University of Waikato, Hamilton. 16pp.

Cover picture: Preparing the instruments for deployment on the wharf. Photos: Ben Stewart.

Reviewed by:	*Approved for release by*
	
Dr. Andrew La Croix	Name
Senior Lecturer	Co-Director
University of Waikato	Environmental Research Institute

EXECUTIVE SUMMARY

A suspended sediment transport model was set up for Ōhiwa Harbour, which was validated against in situ observations collected between 19/4/21 and 17/5/21. Four sediment grain size fractions were modelled; two cohesive (silt) sediment grain size fractions, and two non-cohesive (sand) sediment grain size fractions. Characteristics of these grain size fractions were selected based on a sensitivity analysis and the match of modelled suspended sediment to the magnitude and temporal patterns recorded at the observation stations. Suspended non-cohesive grain size fractions reflect local current strengths at the sites measured, whereas cohesive grain size fractions are advected longer distances by the ebbing or flooding currents.

Sediment loading was input at the freshwater discharge points using loading scenarios provided by the Bay of Plenty Regional Council. Sediment loading was converted to a concentration and discharge, and input into the model as a cohesive sediment grain size fraction. Model scenarios were run for 1 year in blocks of 3 months, using the environmental conditions (discharge, wind, tides) from 2014 as a base-case scenario. Loading scenarios consisted of contemporary, natural, RCP45 and RCP85 conditions. A 7-day model "warm up" period prior to each of the 3-month blocks was discarded.

Suspended sediment concentrations in the Harbour were dominated by resuspension of sediments from the seabed, with the freshwater inputs only contributing a small fraction of the total. Sand eroded and was then accreted around the complex higher-energy entrance region. Finer (cohesive) sediment fractions accumulated preferentially at upper intertidal depths, and in the upper (farthest from the entrance) regions of the Harbour. These regions have much longer residence times, and so cohesive sediment has time to settle out of suspension before the tidal currents can remove them from the estuary. Net accumulation rates were quantified as the change between the initial and final bed levels, divided by the time period of the simulation. Some areas of the Harbour (such as channels) showed no appreciable sediment accumulation but rather consistently eroded, which contributed additional suspended sediment to the model domain.

Linear increases in sediment loading between scenarios caused a linear increase in sediment accumulation within the model domain. However, the total amount of sediment accumulated within the grid was much smaller than the total amount of sediment delivered to the Harbour. This is due to net erosion of some regions within the grid. To isolate the relative contribution of new versus resuspended sediment, accumulation was linearly extrapolated to determine accumulation under zero sediment loading. The baseline accumulation was then removed from each of the sediment loading scenarios to provide an estimate of new catchment-derived accumulation. This analysis suggests that currently 3 times as much sediment accumulates in the harbour relative to natural (pre-European) conditions (1.47 kt/year versus 0.47 kt/year), which could potentially increase to 5.5 and 6 times as much under the RCP45 and 85 scenarios respectively.

The main limitation of the model was lack of knowledge of the parameters needed to set up the sediment model and insufficient spatially-resolved suspended sediment calibration data to determine which settings were most appropriate. These issues are extremely common (and generally unresolved) in sediment modelling in morphologically-complex mixed grain size estuaries like Ōhiwa Harbour.

TABLE OF CONTENTS

Contents

LIST OF TABLES

LIST OF FIGURES

1. INTRODUCTION

Water quality and sediment delivery into New Zealand's estuaries are of ever-increasing national importance. Land use changes across catchments over the last century have been accompanied with elevated sediment loading into coastal waters and a decline in biodiversity and ecological value (Thrush et al., 2004). In the Bay of Plenty Region, where the underlying geology is easily erodible, the delivery of sediment into sensitive receiving environments such as, rivers, lakes and estuaries is a broad management challenge (Vale et al., 2021). National policy around building and implementing water quality and sedimentation limits has recently been introduced under the NZ Freshwater Policy Statement (2020). Regional authorities have therefore been tasked to manage land use and activities affecting freshwater, as well as its effects on receiving environments. This has renewed the urgency to better understand the dynamic processes occurring within coastal and estuarine systems.

In Ōhiwa Harbour, local Māori communities have lived and harvested from the estuary for centuries and it is an important mahinga kai (food gathering place) for shellfish and seafood (Morrison 2007; Paul-Burke et al., 2018). However, the traditional, green-lipped mussel species (kuku or kūtai, *Perna canaliculus*) among other shellfish have struggled to maintain their existence and thrive in the once abundant food basket of Ōhiwa (Paul-Burke et al., 2018; Paul-Burke et al., 2022). Reducing suspended sediment loads within the Ōhiwa catchment and increasing understanding and awareness through the exercise of kaitiakitanga (guardianship) forms part of the sustainable management actions outlined in the Ōhiwa Harbour Strategy (BOPRC, 2014) and freshwater management framework (BOPRC, 2015).

Under changing climate and hydro-meteorological conditions predicted over the coming decades, understanding fundamental processes such as transport and exchange of flows occurring within estuaries will be of increasing importance. Ōhiwa Harbour is one example where increased suspended sediment loads during extreme storm events may have detrimental impacts through the smothering of fauna, reduced water quality, and elevated nutrient loads (Park., 2005, MacKenzie., 2013, Vale et al., 2021). The associated colour of finer terrestrial derived sediments, such as muds and clays, can also be enough to substantially diminish the light quality in estuaries (Cussioli et al., 2020). Large scale single events may therefore be problematic as, once deposited, the sediment can be re-worked through internal processes over time.

Predicted sea level rise associated with climate change is an active area of research and will also impact estuarine environments. However, this may not affect all coastal regions uniformly (Levy et al., 2020) and the coastal response to sea level rises will largely depend on the unique sediment inputs and bathymetric conditions of a particular estuary (Rahdarian et al., 2022). To help understand the past, present and future sedimentation in Ōhiwa Harbour, a recent and co-current sediment study by La Croix (2022) investigated sediment accumulation rates and characteristics through vibro-coring of intertidal regions. Although no rate could be achieved through radionuclide dating, a high level of bioturbation and mixing through the cores were observed. More recently, Bruce (2023) used radiocarbon dating of marine shells and age-depth modelling to constrain sediment accumulation rates over longer timescales (centuries to-millennia). However, this work was challenged by the incomplete nature of the sedimentary record in Ōhiwa Harbour.

The Bay of Plenty Regional Council (BoPRC), together with local iwi groups, have made efforts to reduce sediment loads over the years through measures such as extensive riparian fencing, which has been established along major streams and rivers in the Ōhiwa catchment (MacKenzie 2013, BOPRC.,

2014). The ‘current state’ of Ōhiwa Harbour has been defined for the year 2014 due to the work covered in the Ōhiwa strategy (2014) and the objective in the Council coastal plan that states “sediment accumulation in harbours and estuaries resulting from land use and accelerated erosion is minimised and reduced over time compared to 2014 levels” (Park., 2022 pers. comm.).

Landcare Research (Manaaki Whenua) have recently provided catchment sediment modelling on erosion and suspended sediment loads across the region for a range of land cover, erosion mitigation, and climate change scenarios (Vale et al 2021). This has included the modelling of mean annual suspended sediment loads to a daily time step for streams entering the Ōhiwa Harbour, which is intended for the coupled use with a hydrodynamic model of the harbour (Vale et al., 2021).

The University of Waikato was therefore commissioned by BoPRC to develop a hydrodynamic model to help in the understanding of sediment exchange within Ōhiwa Harbour, and to assess sediment transport & accumulation under different loading and climate change scenarios. This is intended to provide the council with much needed information on setting limits of sediment loads to achieve moderately healthy benthic macrofaunal communities in the harbour and support the implementation of the New Zealand National Policy statement for Freshwater Management 2020 (NPS-FM).

The objectives for this project were to:

1. Set up a hydrodynamic and sediment transport model for Ōhiwa Harbour that is calibrated to measurements obtained from the field (water levels, current velocities/directions, suspended sediment concentrations).
2. Provide the ‘current state’ conditions for the harbour (based on the year 2014)
3. Assess sediment transport and accumulation rates within the Harbour
4. Model sediment loading under ‘current state’, ‘natural state’ and predicted climate change scenarios.

2. STUDY SITE

Situated on the North Island of New Zealand, Ōhiwa Harbour is an estuarine lagoon covering an area of 26.4 km^2 (Figure 1). The harbour is enclosed by two barrier sand spits and is largely intertidal with 83% of its area being exposed sand and mud flats at low tide (Park., 2005). Semi-diurnal tidal currents (spring-neap tidal range of 1.6 – 2.5m) underpin the main exchange process with the ocean. Tidal scouring and channelization of flows occur throughout the harbour, which can be highly dynamic toward the harbour entrance. Wind-waves around the shallow fringes of the harbour also occur and can be steep and choppy, reaching heights of up to 0.5 m (Richmond, 1977). This internal wave climate is directly driven by the predominant wind direction, which can vary between more westerly or northerly flow patterns depending on the El Niño/La Niña phases of the El Niño Southern Oscillation (ENSO) (Richmond., 1984; Julian., 2006). The annual average rainfall is ~1300 mm per year with the wettest months in winter (Chappell., 2013), although climate events can be quite extreme and episodic especially when influenced by El Niño/La Niña phases.

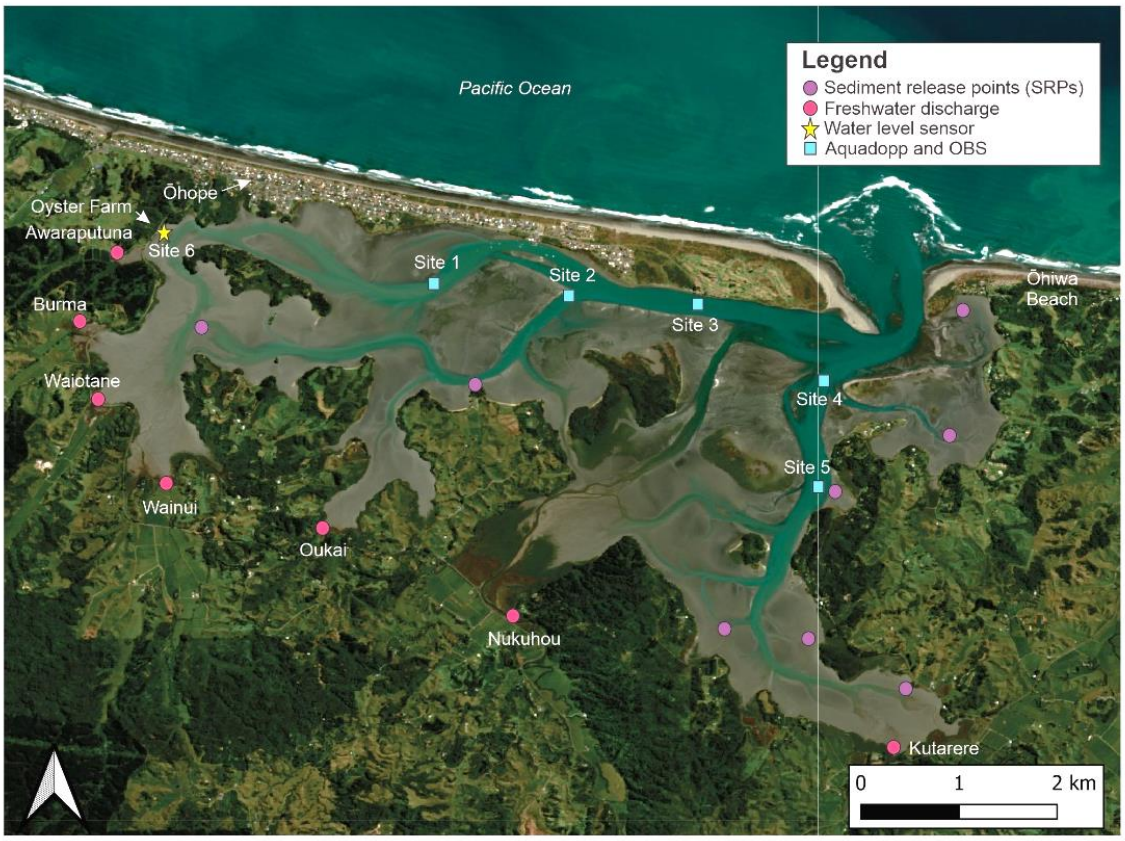

***Figure 1**: Field site including deployment locations and the location of stream inflows (background image is from Sentinel-2 satellite data).*

Freshwater input into the harbour is relatively small and dominated by the Nukuhou River, which has been gauged since 2011 and drains 60% of the harbour catchment (BOPRC., 2014) at an average flow rate of 1.68 m^3/s (maximum recorded is 55.6 m^3/s). Other smaller streams flowing into the harbour include the Awaraputuna, Burma Road, Waiotane, Wainui, Oukai, and Kutarere streams (Figure 1). The catchment area (171 km^2) has regions of steep topography with native forest but also large areas of production forestry and pasture, which are used for dairy farming horticulture and lifestyle blocks (BOPRC., 2014). Catchments across the Bay of Plenty region are prone to multiple erosion processes such as shallow landslides, earthflow, gully and surficial erosion, as well as streambank erosion (Beetham 2012, Vale et al., 2021). Ōhiwa Harbour is also surrounded by steep cliffs comprising approximately 12.5% of the coastline (S. Park, pers. comm.), which are made up of easily erodible sedimentary strata.

The geology surrounding Ōhiwa Harbour is of relatively young volcanic origin, with multiple faults dissecting stratiform sedimentary rocks and tephras (Richmond et al., 1984). The composition of sediment in the upper harbour is dominated by volcanic glass, pumice fragments, and feldspar. The lower harbour is more rich in quartz and feldspar (Richmond et al., 1984, La Croix 2022). Large scale events such as earthquakes, volcanic eruptions, and tsunamis have also provided stepwise changes in sediment budgets to the Rangitaiki Plains, which together with the Motu River, provide a sediment supply to the sand spits at the harbour entrance by offshore littoral drift (Robinson., 2012). Ongoing monitoring work done by the BOPRC in the harbour has shown sediment grain size distributions that are finer / muddier in the upper harbour reaches (Figure 2). This overall grain size distribution within

the harbour is supported by surveys conducted by the National Institute of Water and Atmosphere (NIWA; Bulmer., 2022), illustrating a higher proportion of mud in the channels of the upper western Harbour region (Figure 3). La Croix (2022) also showed that the intertidal perimeter and upper reaches of the Harbour are characterised by fine sediments (Figure 4). These regions of the Harbour comprise clast supported calci-gravel, sands and silts (ripple or bioturbated), and through time these sediments have become muddier (La Croix., 2022).

Land use in the catchment of the harbour consists of 41% pasture, 21% indigenous forest, and 16% exotic plantation (BoPRC, 2018). Most of the streams in the catchment have been fenced. Although monitored nutrient levels are low, intertidal benthic habitat is not in good condition because of the influence of mud (BoPRC, 2018). Three faults run north-south; one to the west through Ohope (the Ohope Fault), one down the centre of the Harbour (Waimana Fault, running just east of Uretara Island) and one to the east down the Waiotahe River (Waikaremoana Fault) (Healy and De Lange, 2014).

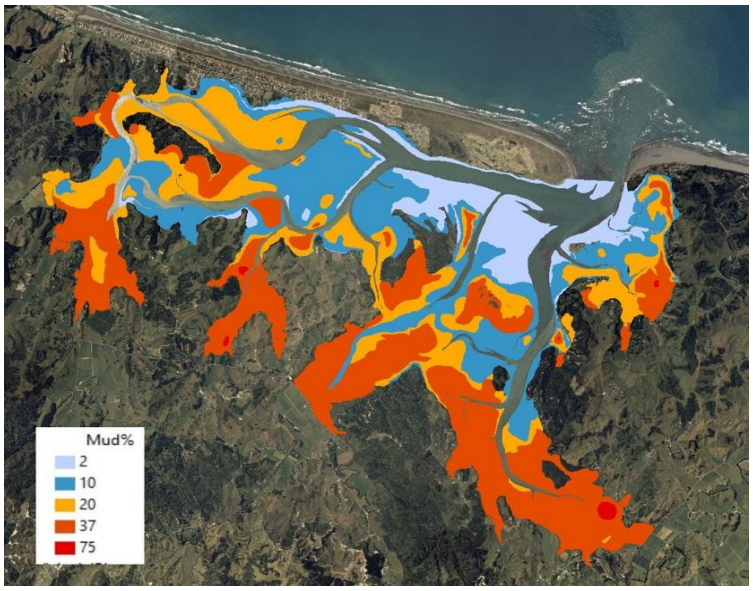

Figure 2: *Particle size distribution map provided by the Bay of Plenty Regional Council.*

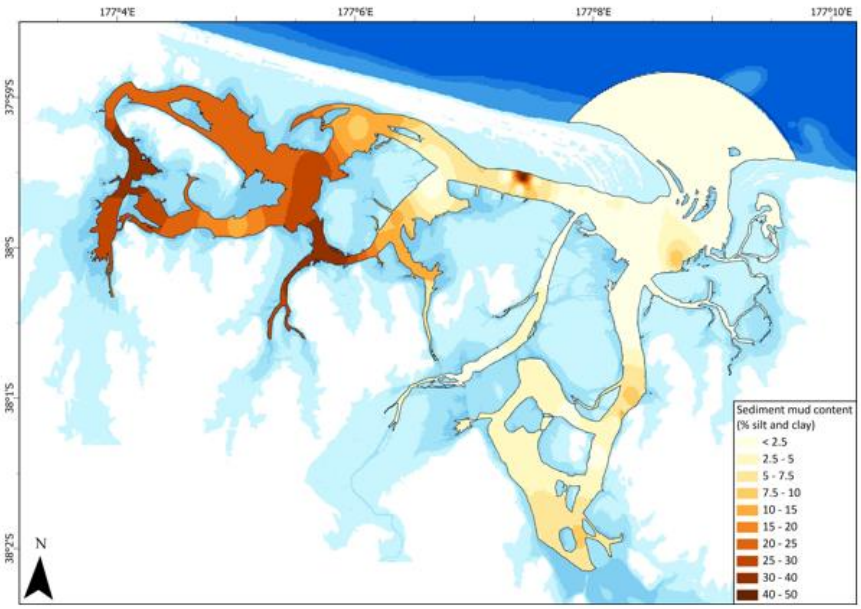

Figure 3: *Percentage mud distribution provided by Richard Bulmer, (pers. comm. 2022).*

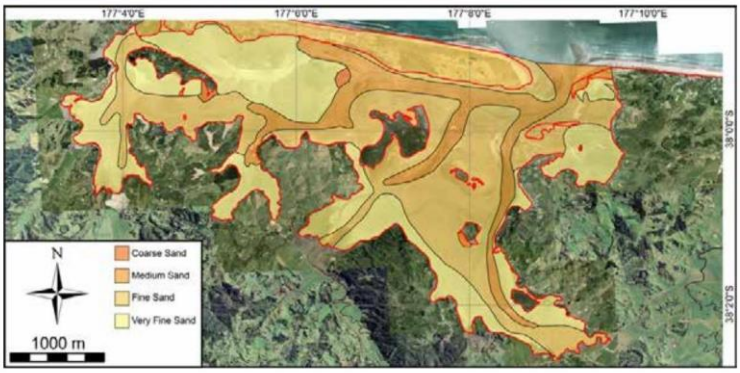

Figure 4: *Mean grain size map reproduced from La Croix (2022), as modified from Richmond et al., (1984)*

3. METHODS

3.1 Field data collection and processing

3.1.1 Hydrodynamic data processing

Hydrodynamic data were collected on 5 separate 'Nortek Aquadopp' instruments which were deployed by scientific divers in the main harbour channels and sub-channels (locations shown in Figure 1) for a 1-month period between the 19/4/21 – 17/5/21. All 'Nortek Aquadopp' velocity data were converted to east-north-up (ENU) coordinates and burst-averaged every 4 minutes with data points being removed when the sensors were out of the water (all instruments were submerged at ~2 m depth or greater during deployment). Instrument orientation/heading was checked and corrected with field measured orientation/heading observations. Pressure data were not corrected for local atmospheric variations over the deployment period. A separate 'LevelSCOUT' pressure and

temperature sensor was also used to measure water levels and the timing of tides in the upper reaches of the harbour (Figure 1). This was placed at a stage height of 2 cm above the mud flat with bed level and instrument pressure being corrected to local water level (in m). This included hourly variations in atmospheric pressure (sourced from Whakatane, NIWA CLIFLO, 2022) being subtracted from the sensor data, which was fully exposed at low tide. All data and timestamps from instruments were interpolated with modelled data timestamps for calibration.

3.1.2 Sediment calibration

All of the 5 'Nortek Aquadopps' that were deployed in the harbour were fitted with 'Campbell Scientific' optical backscatter sensors (OBS3+). The measured optical backscatter, which is measured in voltage/counts on the Aquadopp instruments, was used to estimate the suspended sediment concentrations (SSC mg/L) in the water column. OBS3+ sensors emit infrared light into the water column and measure the backscattered light intensity reflected from the suspension of particles. Previous investigations have successfully used linear regression to convert measured light intensity counts to SSC (mg/L) using lab-based methods to calibrate instruments with sediments from the field (MacDonald, 2009; Lovett, 2017).

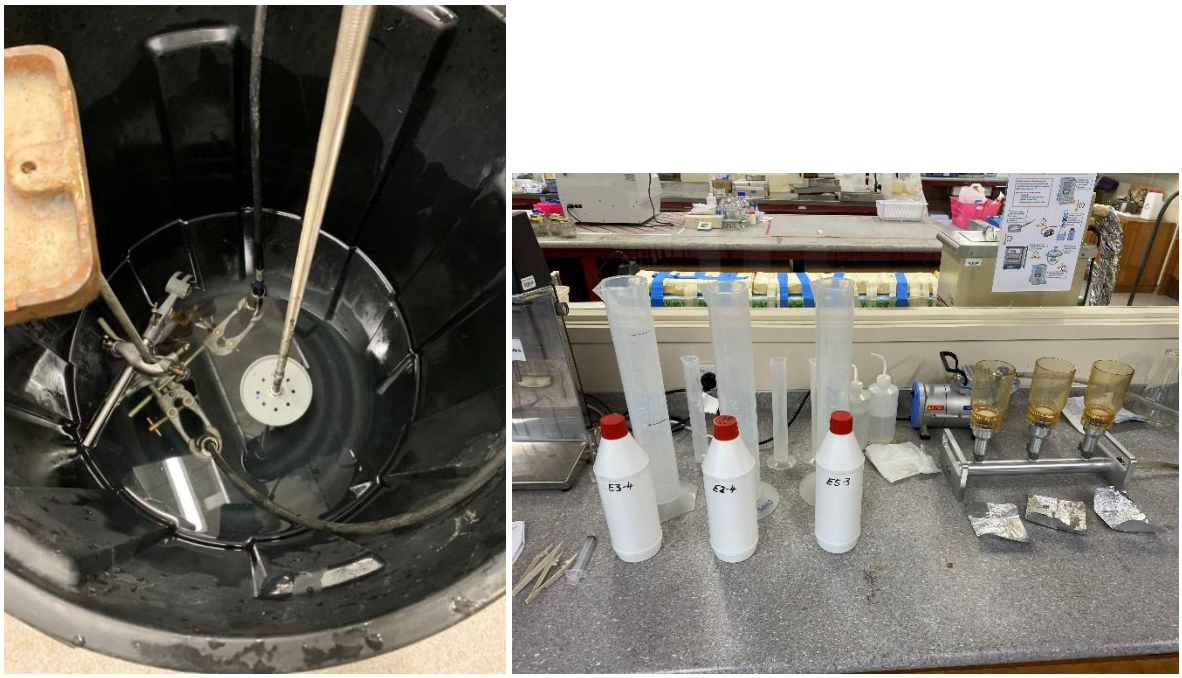

Figure 5*: Photos of calibration set up. (Left panel) The calibration tank showing the OBS (the back cable with clamps is the OBS3+) and stirring mechanism (metal post). (Right panel) The filtration system.*

The OBS3+ sensors used during the field deployment were calibrated in the laboratory using a mixture of native sediments collected through extensive grab sampling across the intertidal regions of Ōhiwa Harbour (La Croix, 2022). A 60L capacity dark bucket was used with a stirring rod to ensure that sediment that was added to the bucket was well-mixed and kept in suspension for as long as possible. Care was taken on the positioning of the stirrer and the OBS3+ sensors (Figure 5 - left panel) to not produce excessive bubbles or swash which may interfere with backscatter readings. Sediment samples from intertidal areas near each individual sensor deployment were mixed and sieved using a 62.5 μm mesh. A dummy OBS3+ sensor was used as a live monitor of counts on a survey laptop to roughly estimate the range which was observed in the field and how much sediment to expect to add. This ensured that sediment was added in a continuous stepwise manner. Five water samples were collected from start to finish for each sensor, which covered the range of counts

measured in the field. Each grab sample was manually logged and timestamped while the instrument was recording continuously. The water samples were then filtered using Whatman glass microfiber filters (GF/C diameter 47 mm). Filters were previously prepared by being dried for 24 hrs at 105°C and weighed. A known concentration of sample (200ml) was washed through the filters with distilled water (Figure 5 - right panel), dried in the oven for 24 hours at 105°C and weighed again to calculate SSC as the mass/volume (mg/L).

The measured SSC, which was derived from the native sediment lab samples, was plotted against the OBS3+ voltage/counts to create a regression curve for calibration. Figure 6 illustrates the high r^2 values (all over 0.97), fitting coefficients and confidence bounds across all sensors and indicates that a good calibration between SSC (mg/L) and instrument voltage/counts was achieved. The fitting coefficients were then applied in a regression model to each of the 5 OBS3+ data obtained over the field deployment period to achieve high resolution and dynamic in field SSC concentrations (mg/L) (Appendix 5).

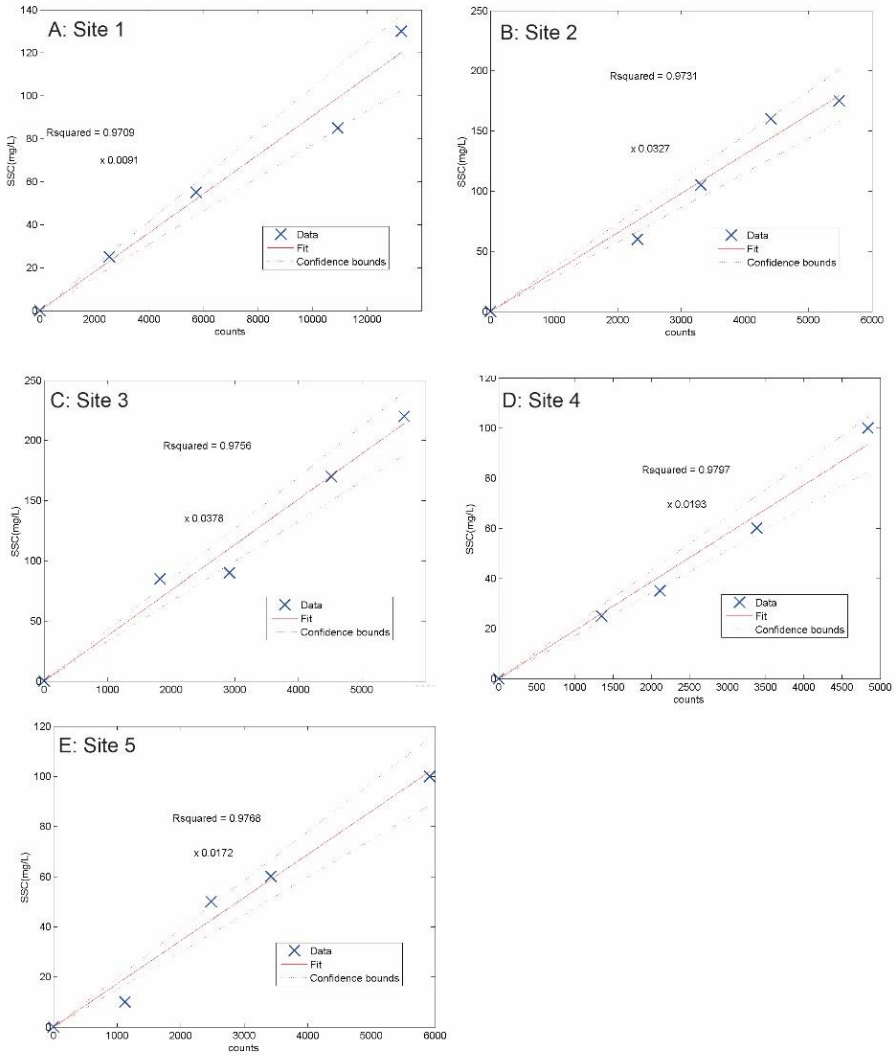

***Figure 6**: Results of laboratory sediment calibration. The fitting coefficient and r-square are noted on each panel.*

3.2 Model setup

The modelling framework used for this study was the Delft 3D-FLOW model, which is open-source software provided by Deltares. These models have been well established across a growing number of studies and are freely available, with a large international base of users. The governing equations used in the Delft 3D-FLOW model and associated modules are described in further detail in Deltares (2017, 2018) and Lesser et al. (2004). Essentially the model solves the unsteady shallow water equations and was developed specifically for regional studies, and thus can be applied in lakes, estuaries, shallow seas, and rivers. For Ōhiwa Harbour, we have chosen to use a 2D depth-averaged model, mainly due to the shallow, mixed nature of the harbour (mean depth ~2m), the small freshwater input and the benefit of requiring lower computational demand and greater simulation efficiency. The major stages for setting up and running the numerical models included:

- Setting up model grid and bathymetry.
- Forcing the model hydrodynamics with tides (at open boundaries), river discharge (at closed boundary points) and winds (time-varying across the model grid).
- Calibration to observed field water levels, current speeds and directions.
- Sediment transport model calibration to field data using various sediment calibration parameters and variations in sediment type (coarse sand, silt, fine mud etc).
- Timeseries of river and stream inputs into the harbour.
- Scenario testing using variations in the specified hydrodynamic forcings and sediment inputs.

3.3 Bathymetric grid setup

Due to the spatially varying and dynamic bathymetry across Ōhiwa Harbour, multiple data sources were used when creating the bathymetric grid for the model domain. This included LiDAR (Light Detection and Ranging) data (2015) created from the Bay of Plenty 1m digital elevation model (Figure 7) for detailed intertidal topography. To capture the bathymetry of the dynamic channels at the harbour mouth, Bay of Plenty Regional council commissioned Discovery Marine Limited (DML) to conduct a detailed single beam survey between the 2-3rd of June 2021 (Figure 8). This was combined with detailed boat survey data (RTK and Multibeam) in the channels of the harbour by the University of Waikato (Dean Sandwell and Megan Raiapa) in 2019 (Figure 9). LINZ hydrological Chart NZ 542 and LINZ Bay of Plenty depth contours and sounding points (2020) were used for offshore regions of the domain. All data sources were converted from their respective datums and corrected to mean sea level. This resulted in an interpolated bathymetry used for calibration and the hydrodynamic model (Figure 10A).

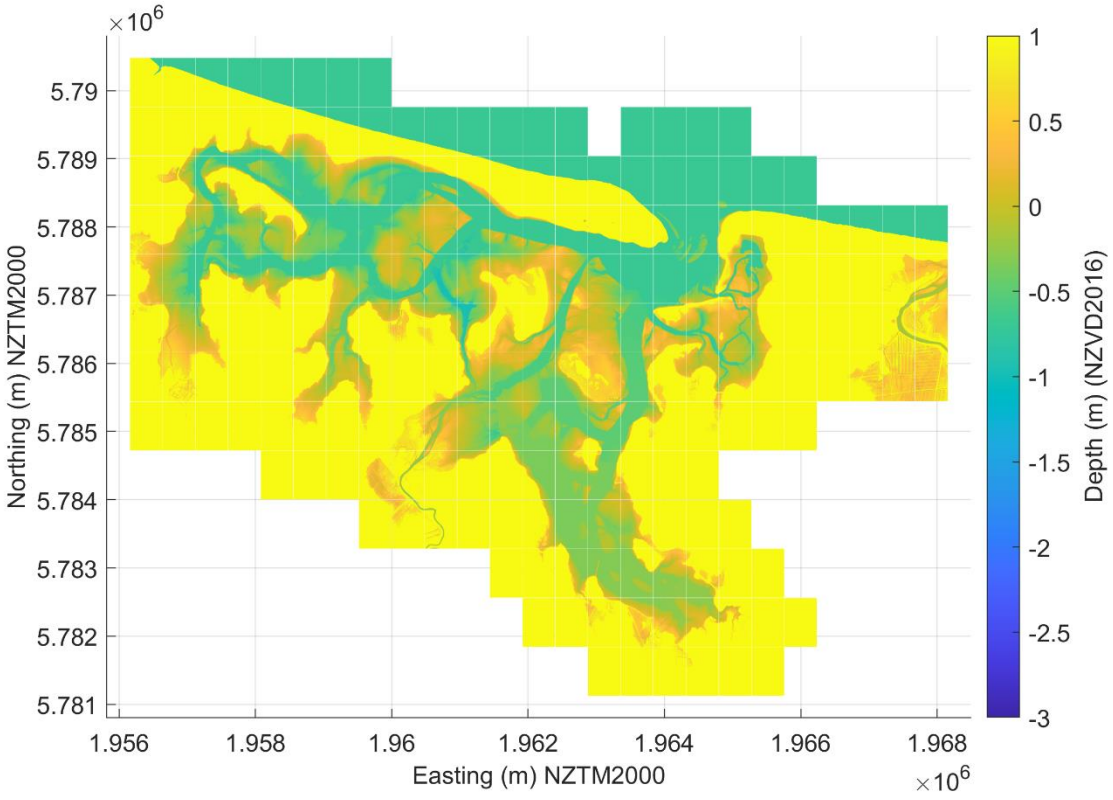

Figure 7: *LiDAR map of Ōhiwa Harbour, created from the Bay of Plenty Tauranga 1m DEM 2015 available for download from Land Information New Zealand.*

A 2D hydrodynamic model was created with a single domain 20 × 20 m rectilinear mesh grid (Figure 10B). This resolution was chosen to resolve the complex channels, islands and sub-estuarine constrictions within the harbour and included a total of 128,242 grid elements. The three open ocean boundaries were set close enough to the coast to capture the ebb jet and return flow out of the harbour entrance (~2.3 km offshore) but not far enough to capture detailed offshore oceanic processes (may be nested to coarser oceanic modelling in future estuarine / shelf work). Grid cells over low-lying areas and around the coastal perimeter were included for sea level rise and inundation modelling scenarios.

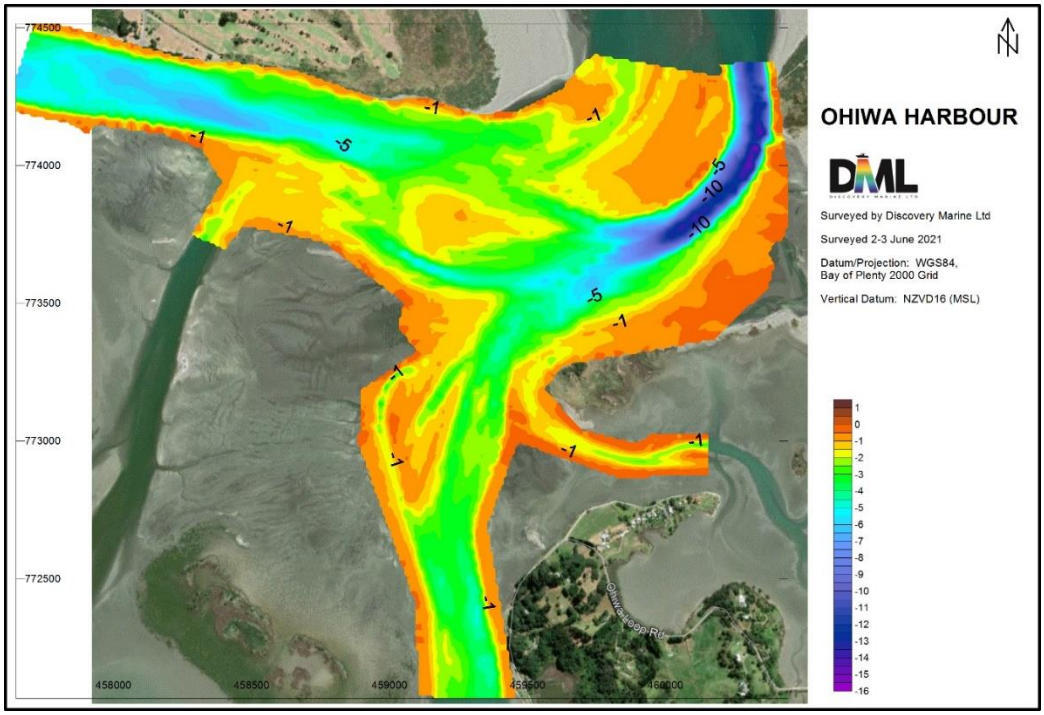

***Figure** 8: Bathymetric survey undertaken by surveying company Discovery Marine Ltd (DML) in June 2021.*

***Figure 9:** Extent of bathymetric survey undertaken by Dean Sandwell and Megan Raiapa at the University of Waikato in 2019.*

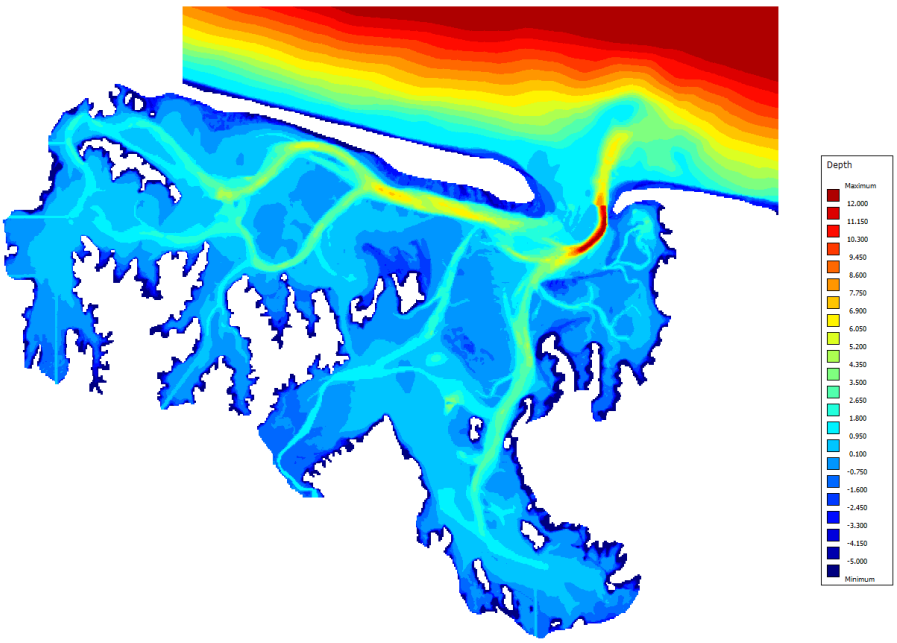

B

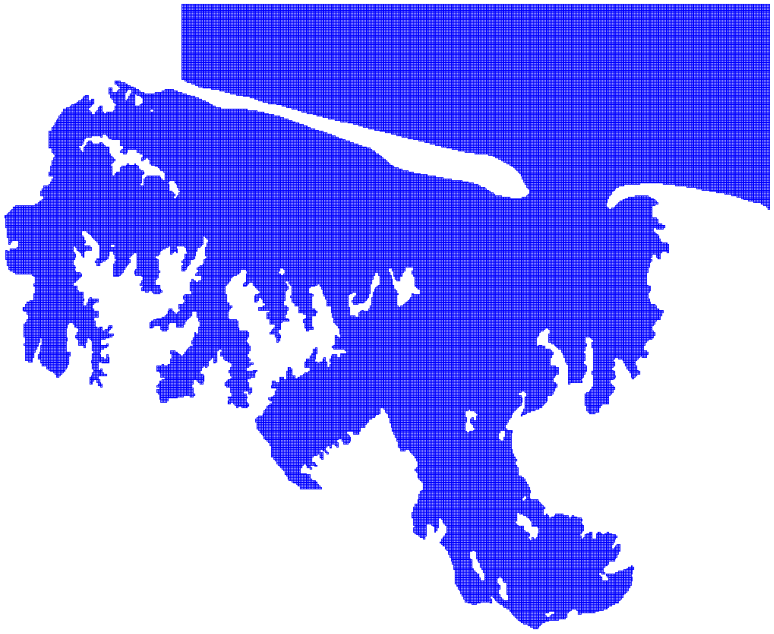

Figure 10: *A: Model bathymetry (depth relative to mean sea level). B: Model grid (each grid cell is 20 m by 20 m).*

3.3 Model boundary timeseries preparation and forcing

3.3.1 Wind, stream inflows and sediment input data

Wind speed and direction can often have an influence on circulation patterns, especially in shallow estuaries. Wind speed and wind direction timeseries were created from weather information extracted from the Bay of Plenty Environmental data portal (2022) at Ohope spit golf course (ML293777) for simulation years after 2015 and Edgecumbe (JL671469) for years prior to 2015. These timeseries were input as hourly data which was applied uniformly across the whole domain.

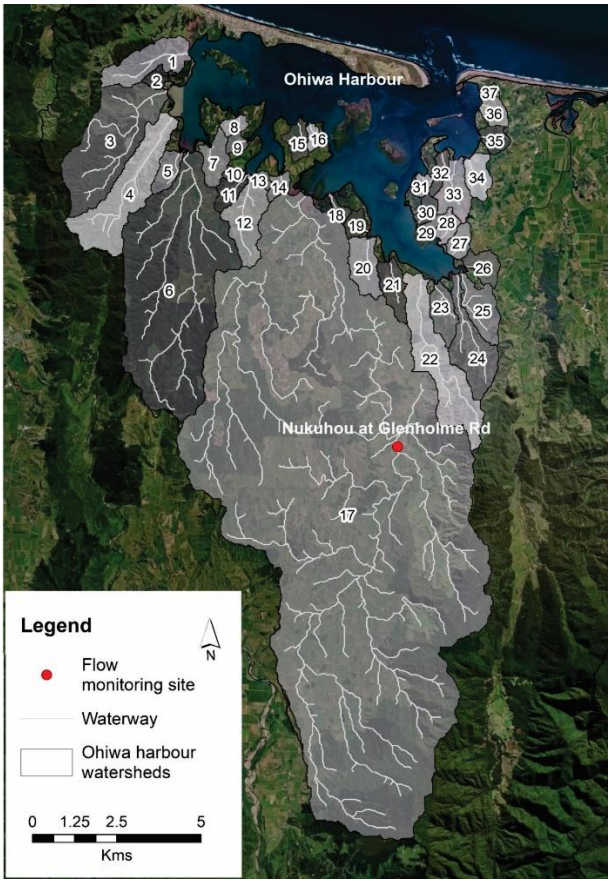

***Figure 11**: Catchment map used in SedNetNZ modelling by Manaaki Whenua (Figure 8 in Vale et al., 2021)*

Freshwater discharge inputs to the model were defined as cell points to cover all the major streams and catchment watersheds feeding into the harbour (Figure 1 & Figure 11). The BOPRC has one continuous flow monitoring site at Nukuhou River which provides high frequency discharge rates (m^3/s). Due to the sparse flow data from other significant streams and the similarities in rainfall across catchments, the Nukuhou flow monitoring site was used as a proxy to estimate the flows of all the major streams entering the harbour. The annual average flow and flood rates (m^3/s) predicted from a NIWA/ CLUES modelling study (Collins and Semadeni-Davies., 2015) as well as spot measurements from BoPRC (2016) helped set the appropriate scaling factor and ensure predicted values were within a sensible range of flow rates. Figure 12 illustrates an example of the flow timeseries generated using this method, with the full outputs for all the major streams (including the Awaraputuna, Burma Road, Waiotane, Wainui, Oukai, and Kutarere streams) presented in Appendix 2

Sediment loading values into the model were derived from SedNet NZ modelling work carried out by Manaaki Whenua (Vale et al., 2021). This work calculated the Ōhiwa daily sediment load ($t\ day^{-1}$) across 37 Ōhiwa Harbour inflows and catchment areas based on unique NZ segment numbers (Figure 12), and included erosion processes, landslides, and earthflow movements over each of the watershed areas. Due to the large number of inflows modelled across the Harbour, catchment regions (as shown and numbered in Figure 11) were aggregated for the hydrodynamic simulations (Table 1). Here we assume that very small catchments shown in Figure 11, were essentially similar to direct cliff supply. There is no simple functionality in Delft3D to model actual cliff loading. So the sediment loading was input as stream and river inputs and smaller catchment points as “diffuse cliff erosion” input points based on that watershed area. For example, ID 15 and 16 provided a single “cliff” erosion discharge point for the SED7 input. Loadings were converted from $t\ day^{-1}$ to an input concentration for the

model in kg/m^3 by dividing the loading by the relative daily stream flow rate (m^3/s). For "cliff erosion" input points, a trickle discharge rate of 0.01 m^3/s was applied, so that the suspended sediment multiplied by the discharge would equal to the correct loading. These cliff points were input into the channels of the model (Figure 1) mainly to make sure that the discharge was connected properly into the model (drying and flooding of cells can strand points that are really shallow and at the edge of the domain). Although these cliff erosion points most likely providing an underestimated value, it does give some idea of the other diffuse process providing sediment into the estuary. These diffuse inputs are traditionally difficult and challenging to include in hydrodynamic modelling yet may provide important unknown contributions. Different sediment loading inputs were used for different model scenarios which included, (1) contemporary state (calibration runs and 2014 contemporary scenarios) (2) natural state and (3) climate change scenarios (median RCP 45 and 85 mid-century).

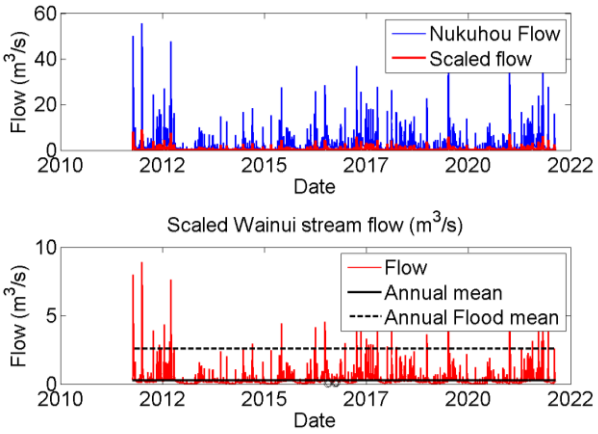

Figure 12: *Example of discharge timeseries for Wainui stream (all other plots are in Appendix 2).*

Delfd3D models sediment transport in two different ways depending on whether the sediment is cohesive or non-cohesive. It can model multiple fractions, but each fraction modelled increases computation time significantly. Based on the field calibration (see below), we elected to use 2 cohesive fractions and two non-cohesive fractions. The two cohesive fractions reflect the combined effect of resuspended legacy sediments in the harbour, and any new sediment introduced into the model at discharge points. Non-cohesive sediment is modelled by setting parameters such as median grain diameter and bed density. The critical bed shear stress for erosion is calculated internally from the grain size. Conversely, the cohesive fraction is modelled by setting the fresh and saline settling velocity, the critical bed shear stress for erosion and the critical bed shear stress for deposition, bed density and the erosion parameters. These are very difficult to measure, and instead, we used the match between observed and the modelled suspended sediment concentrations to infer the optimal settings for these. The result was to use a saline settling velocity of 0.00015 cm/s for the first mud fraction (which was also the one used to model sediment loading), and 0.0001 cm/s for the second mud fraction, which was used to model the accumulation of very fine sediment in the upper reaches of the model domain. When sediment is deposited in an estuary by fluvial input, tidal asymmetry and settling lags tend to sort the sediment, moving the finest fractions to the innermost estuary, and the coarser fractions seaward. This was also the setting which best approximated the calibration data (discussed in more detail below).

Table 1: *Aggregated sediment loading points (stream, river, cliff erosion) for model input. The location of these points are shown in Figure 1. Note 'cliff erosion' is to denote very small catchments, where model discharge points have been modelled using a trickle feed discharge of 0.01 m^3/s (see text for more detail).*

Name	ID	Input Type
Awaraputuna	1	stream
Burma Rd	2,3	stream
Waiotane	4	stream
Wainui stream	5,6,7	stream
SED5	8	cliff erosion
Oukai	9,10,11,12,13,14	stream
SED7	15,16	cliff erosion
Nukuhou	17,18	river
SED9	19,20,21	cliff erosion
Kutarere	22,23	stream
SED11	24,25,26,27	cliff erosion
SED12	28,29,30	cliff erosion
SED13	31	cliff erosion
SED14	32,33,34,35	cliff erosion
SED15	36,37	cliff erosion

3.3.2 Tidal Ocean Boundaries

The open ocean boundary was forced using the 13 main harmonic tidal constituents (M2, S2, N2, K1, O1, Q1, L2, P1, MU2, T2, K2, NU2, 2N2) derived from the NIWA tide forecaster model (Walters et al., 2001). These were applied as an amplitude and phase at the corners of the outer open boundaries as astronomic forcing, with the model recreating the water level at this boundary from these constituents depending on the period over which the model is run. A Thatcher-Harleman time lag of 120 minutes was applied to the right-side open boundary running perpendicular to the coastline.

3.4 Tidal model calibration and verification

The hydrodynamic model calibration process first involved test runs with default bottom roughness coefficients (the Chézy parameter) and verification of the bathymetry, which was done by comparing model outputs of water level and current sensors. This initially involved a check of the timing and tidal amplitudes of water levels to confirm that the channels were well captured in the model. Poorly defined channels and poor interpolation can block the tidal wave from reaching areas in the model domain. Checking of bathymetry in areas of steep gradients and where data interpolations occurred was undertaken. Additional smoothing was applied in areas to ensure hydrodynamic continuity and that water was able to flow freely. The flow of stream inputs across intertidal areas also needed to be manually channelled out to ensure water would connect between the discharge point and the main channels. These are often dynamic meandering channels, however for some stream points in this model a simplified channelisation was performed.

Once initial tidal and water level behaviour was verified, a suite of uniform Chézy values (75,65,55,45) were applied to give a first idea about how the roughness affects the current speeds and behaviour of the model. Higher values provide less friction and increase water flows, whereas lower values provide more friction and therefore a slower water flow. From here a detailed calibration was undertaken which involved creating and adjusting a spatially varying Chézy bottom roughness map (Appendix 1). This was created by attributing depth values varying over channels and intertidal areas with associated Chézy values. Deeper offshore regions and channels had a value of 60–70 while shallow and intertidal mud flat areas had values ranging from 90–50 with mangrove and elevated vegetated areas reducing to below 40 to 1. The final roughness map chosen for calibration was the one which resulted in the best overall calibration statistics across all measurements. The improved model

calibration of higher Chézy values (less friction) on the mudflats likely demonstrates an interesting sheet flow effect with the tides which occurs in muddy environments (Hortsman et al., 2021).

Other parameters used in calibration of the final model were the horizontal eddy viscosity (set to 1 m^2/s), gravity (9.81 m/s^2), density (1025 kg/m^3) and the time-step which was 0.2 (min). Field observations recorded with Aquadopp and logger sensors over the month-long deployment (19/4/21 – 17/5/21) were used to calibrate the current speeds (Figure 13), directions (Figure 14) and water levels (Figure 15). An overview of the calibration statistics was calculated and demonstrated an "excellent" to "good" category across all parameters (Table 2). These were done using standard model skill tests (described further in Appendix 1).

***Table 2**: Summary of calibration statistics. MAE: Mean absolute error; RMSE: Root mean square error; BSS Brier skill score (equations are provided in Appendix 1). The green results are 'Excellent' whereas the red result is 'poor'.*

	Speed (m/s)					Direction (degrees - 0 -360)					Water levels (m)					
Statistic	1	2	3	4*	5	1	2	3	4*	5	1	2	3	4	5	6
		-	-				-			-		-	-		-	-
Bias	0.00	0.01	0.01	0.14	0.01	0.05	21.26	-2.98	9.79	17.19	0.01	0.01	0.03	0.03	0.03	0.02
MAE	0.07	0.08	0.09	0.15	0.10	15.62	27.49	14.18	29.75	24.65	0.13	0.13	0.13	0.15	0.13	0.09
RMSE	0.10	0.10	0.11	0.20	0.13	41.30	48.62	41.25	61.83	53.25	0.16	0.15	0.15	0.18	0.16	0.13
BSS	0.59	0.66	0.66	-0.16	0.69	0.78	0.71	0.79	0.56	0.66	0.91	0.92	0.91	0.88	0.91	0.92

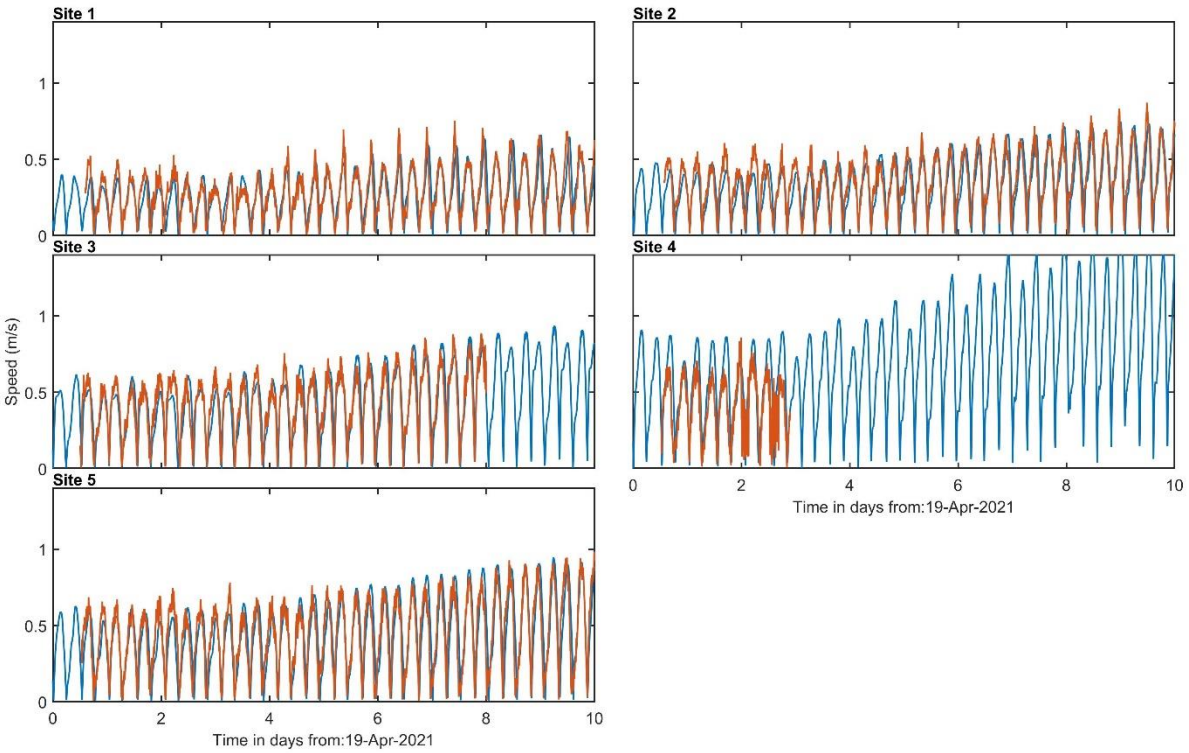

***Figure 13**: An example section of the current speed calibration at each site. The red line is the observations, and the blue line is the model output at each site. Sites 3 and 4 were buried by sediment early in the deployment. The full deployment period is shown in the Appendix 1, (Figure A1: Observed speed (red) and modelled speed (blue) at the sites shown in*

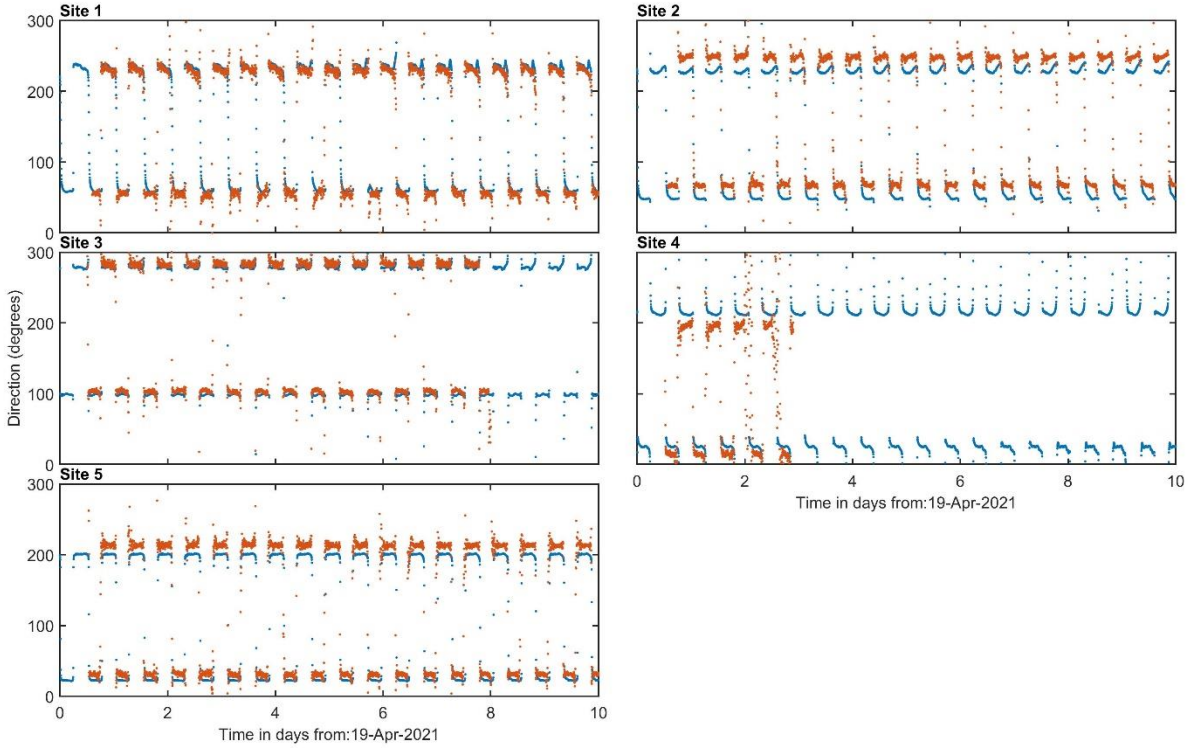

Figure 14: *An example section of the current direction calibration at each site. The red line is the observations and the blue line is the model output at each site. The full deployment period is shown in the Appendix 1, (Figure A2: Observed direction (red) and modelled direction (blue) at the sites shown in*

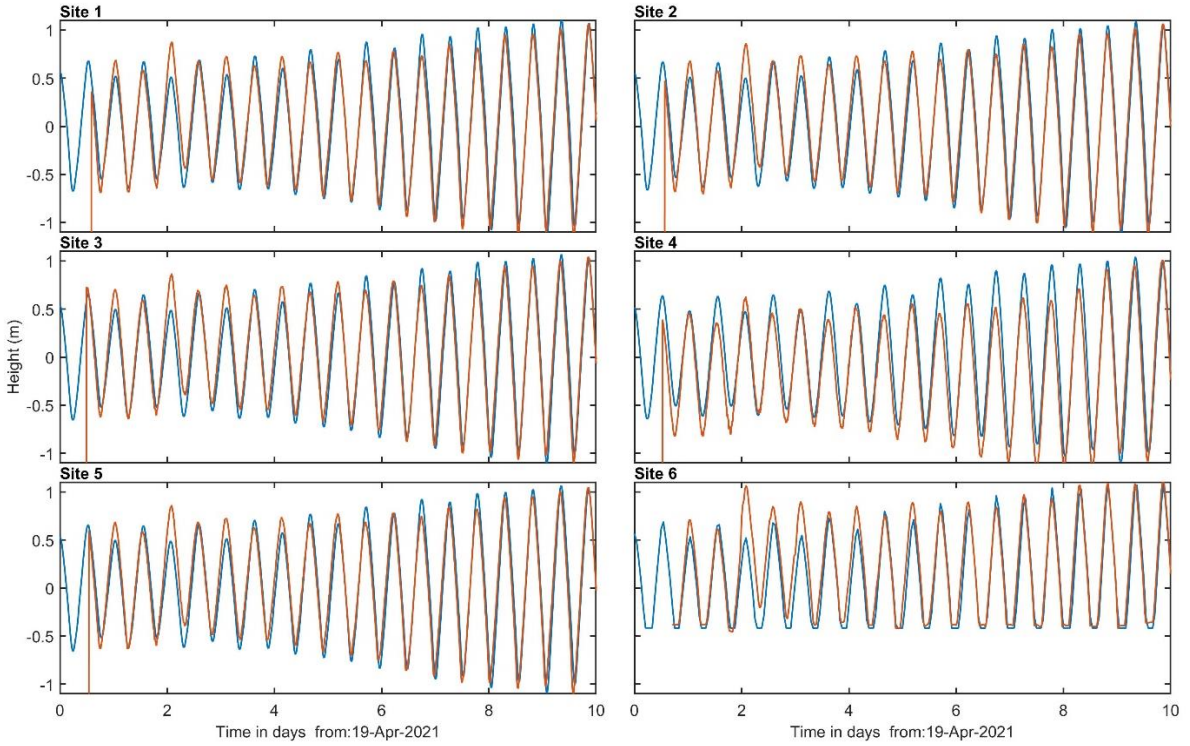

Figure 15: *An example section of the water level calibration at each site. The red line is the observations and the blue line is the model output at each site. The full deployment period is shown in the Appendix 1, (Figure A3: Observed waterlevel (red) and modelled waterlevel (blue) at the sites shown in .*

3.6 Sediment model calibration and sensitivity

There were multiple stages and a wide range of parameters involved in setting up the calibrated sediment transport model. Having high resolution and continuous suspended sediment concentrations (SSC mg/L) measured by the 5 calibrated OBS3+ sensors provided a highly valuable and somewhat unique advantage in the calibration procedure. Measurements of sediment texture by La Croix (2022), BoPRC, and Richard Bulmer (pers. comm. 2022) informed the sediment types to input in the model as an initial bed sediment composition. This initial sediment composition was assigned coarse sand in the offshore region and entrance, coarser sand and mud in the southern channel and multiple layers of mud layers in the upper reaches and tidal flats of the harbour (Figure 16). Suspended sediment concentration was highly sensitive to the relative distribution of each of these sediment fractions. The sandier fractions responded to local current speeds, so maximum suspended sediment occurred when the maximum flood and ebb currents occurred at each site. Conversely, mud could get advected long distances, so maximum suspended mud concentrations at a site, were associated with the arrival time of mud either inland (for ebbing tide) or seaward (for flooding tide) of a site. Figure 17 shows an example of suspended sediment extracted from the model plotted at the 4 sites shown in Figure 16. For example, mud was dominate at site 4 on outgoing tides and fine sand dominate on incoming tides at site 2 (Figure 17). To assess model performance, the different compositions for each individual site were summed (total SSC) and then compared to the SSC (mg/L) measured in the field until the best match in tidal timing and concentration was achieved.

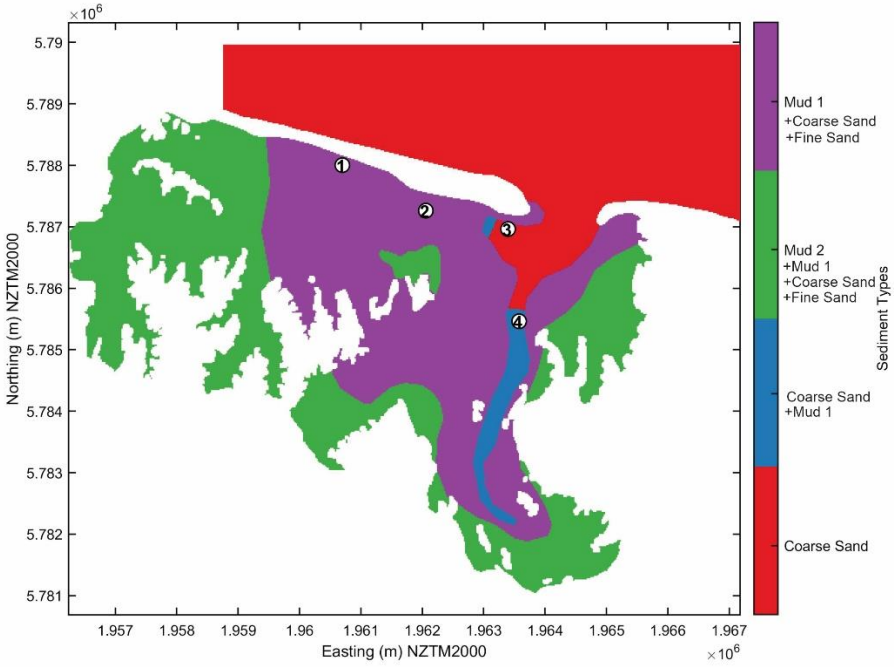

Figure 16*: Initial bed sediment composition showing the distribution of the 4 sediment types used in the model (fine sand, coarse sand and two mud fractions). The area with mud fraction 2 also includes mud fraction 1. The area with coarse sand occurs everywhere in the grid. The fine sand occurs in the area marked fine sand and the area marked coarse sand. The circled numbers correspond to the location where the example timeseries plotted in Figure 17 are extracted (where 1 is the top panel and 4 is the bottom panel).*

A sensitivity analysis was conducted to test the effect of different parameters on the total SSC (mg/L) result. A suite of model runs with changes (increase/decrease) to different parameter values was prepared and analysed. This resulted in an output at each site. The full deployment of mean values with standard deviations and relative changes for each site including the difference from the mean measured SSC (mg/L) over the calibration period (Figure 18). The setup of parameters used for these runs are shown in Table 3. This included variable settling velocities, critical bed shear for erosion, dry bed density, specific density, and the addition of non-cohesive sediments (D50). Stream inputs of sediments had relatively little effect on the calibration with orders of magnitude increases required to have any significant effect on concentrations at the calibration sites. This demonstrated that internal processes and the type/timing of sediment being advected within the harbour had the biggest influences on concentrations over the calibration period. The best model assessed from the sensitivity tests resulted in Model G, which was used as the base for the sediment transport model. Figure 19 shows the comparison between this model setup and the measured SSC (mg/L) over the calibration period. A good agreement between the modelled and observed datasets was achieved, providing confidence for further model scenarios and sediment simulations. Waves were not included for this study; however, it is likely they would also influence the observed concentrations.

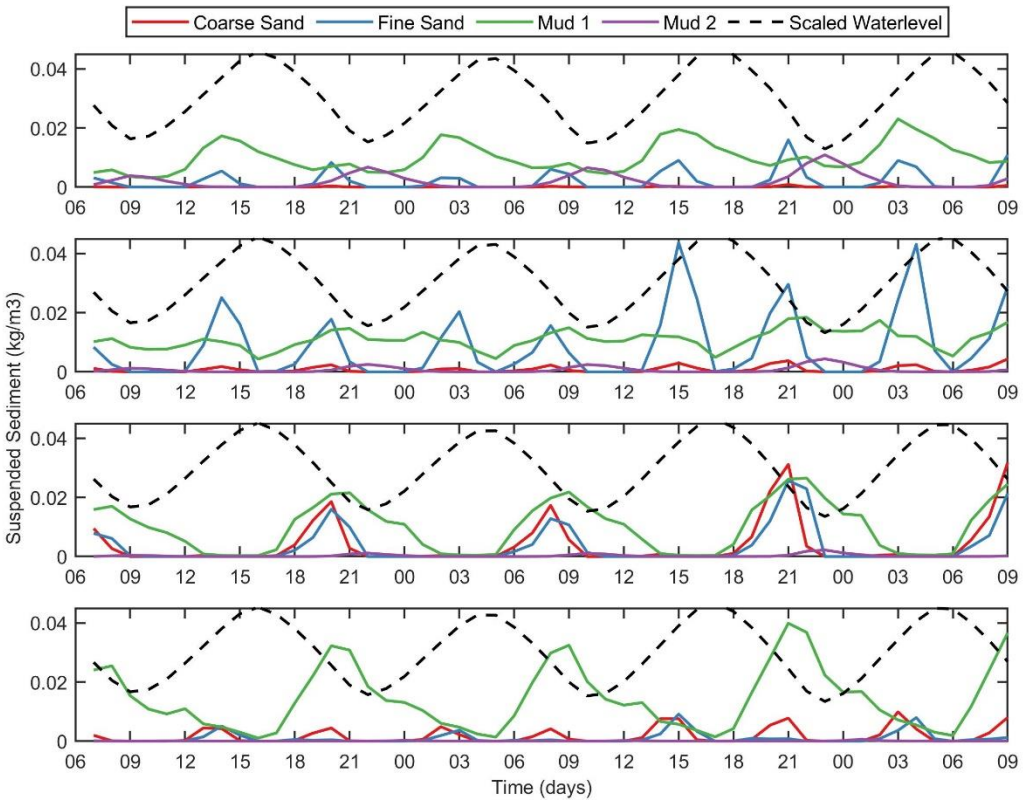

Figure 17: *Example timeseries of the 4 fractions of sediment used in the model. The panels correspond to the locations plotted in Figure 16: Initial bed sediment composition showing the distribution of the 4 sediment types used in the model (fine sand, coarse sand and two mud fractions). The area with mud fraction 2 also includes mud fraction 1. The area with coarse sand occurs everywhere in the grid. The fine sand occurs in the area marked fine sand and the area marked coarse sand. The circled numbers correspond to the location where the example timeseries plotted in Figure 17 are extracted (where 1 is the top panel and 4 is the bottom panel)., with the top panel corresponding to site 1.*

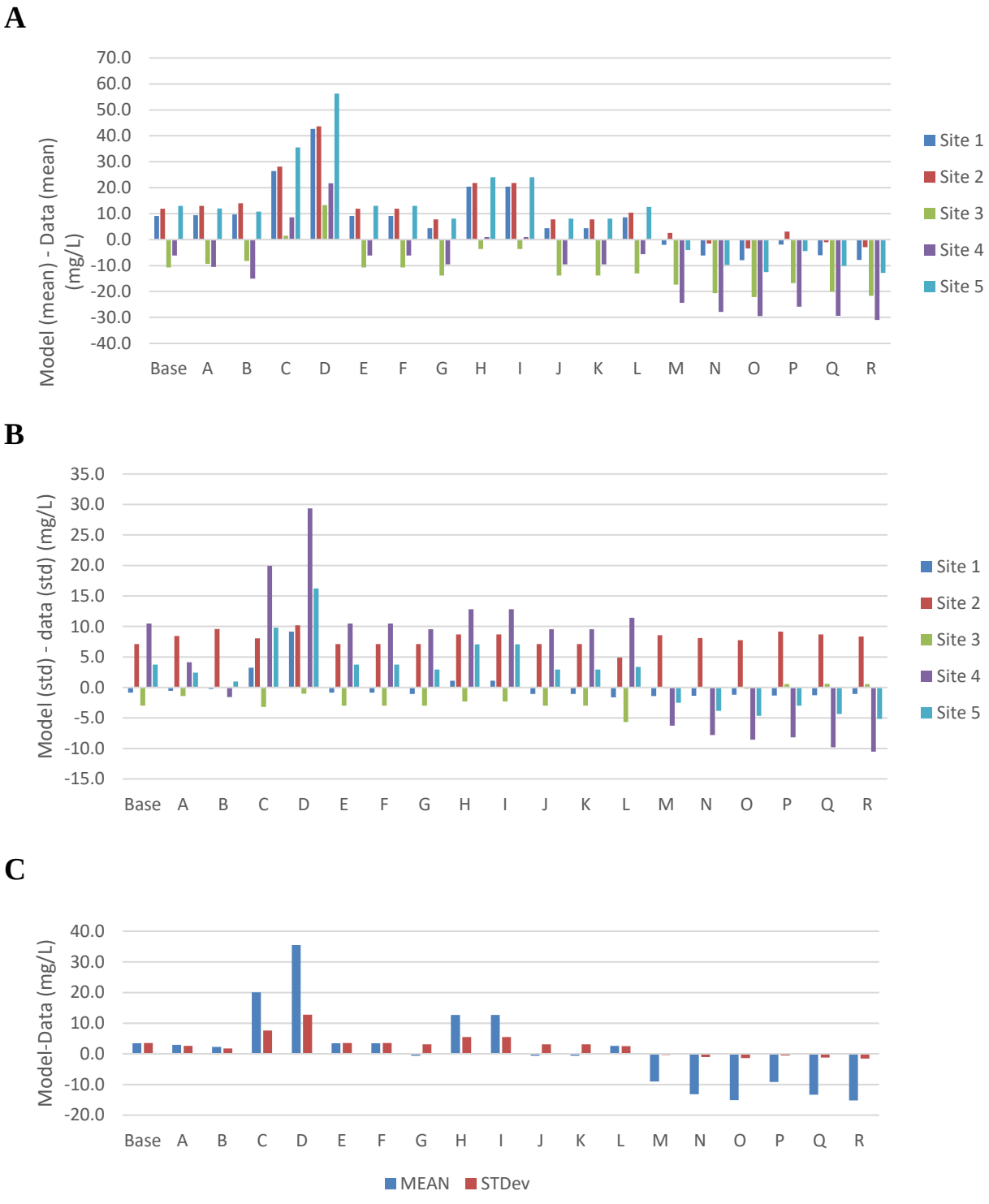

***Figure 18**: The results of sensitively analysis. Panel A: The difference between the mean model output and the mean of the observations at each site. Panel B: The difference between the standard deviation of the model output and the standard deviation of the observations at each site. Panel C: The blue bars correspond to the difference between mean model output and mean observations over all sites, averaged over all 5 sites (the mean of the values shown in Panel A). The red bars correspond to the difference of the standard deviation of model output and the standard deviation of the observations over all 5 sites (the mean of the values shown in Panel B).*

Table 3: *Set up of model runs used for sensitivity runs.*

			Base	A	B	C	D	E	F	G	H	I	J	K	L	M	N	O	P	Q	R
Model Settings																					
reference density for hindered settling			1600	1600	1600	1600	1600	1600	1600	1600	1600	1600	1600	1600	1600	1600	1600	1600	1600	1600	1600
specific density			2650	2650	2650	2650	2650	2650	2650	2650	2650	2650	2650	2650	2650	2650	2650	2650	2650	2650	2650
dry bed density			500	500	500	1000	1500	500	500	500	500	500	500	500	1000	500	500	500	500	500	500
fresh settling velocity			0.1	0.1	0.1	0.1	0.1	0.15	0.05	0.1	0.1	0.1	0.1	0.1	0.15	0.1	0.1	0.1	0.1	0.1	0.1
saline settling velocity			0.1	0.1	0.1	0.1	0.1	0.1	0.1	0.15	0.05	0.1	0.1	0.15	0.1	0.15	0.2	0.25	0.15	0.2	0.25
critical bed shear for erosion			0.1	0.1	0.1	0.1	0.1	0.1	0.1	0.1	0.1	0.05	0.15	0.15	0.1	0.15	0.2	0.25	0.15	0.2	0.25
Non Cohesive																					
D50			350	450	550	350	350	350	350	350	350	350	350	350	350	550	550	550	600	600	600
Average Suspended Sediment (mg/L)		**FIELD**																			
Site 1	MEAN	24.6	33.7	34.1	34.4	51.0	67.2	33.7	33.7	29.0	45.0	45.0	29.0	29.0	33.2	22.6	18.5	16.7	22.7	18.6	16.8
	STDev	13.6	12.8	13.1	13.4	16.8	22.8	12.8	12.8	12.6	14.7	14.7	12.6	12.6	12.0	12.2	12.3	12.4	12.3	12.4	12.6
Site 2	MEAN	24.5	36.4	37.5	38.5	52.6	68.2	36.4	36.4	32.3	46.3	46.3	32.3	32.3	34.9	27.1	23.0	21.1	27.6	23.5	21.6
	STDev	12.6	19.8	21.1	22.2	20.7	22.8	19.8	19.8	19.8	21.3	21.3	19.8	19.8	17.6	21.2	20.7	20.4	21.8	21.3	21.0
Site 3	MEAN	43.3	32.5	33.9	35.0	44.7	56.5	32.5	32.5	29.4	39.7	39.7	29.4	29.4	30.2	25.9	22.6	21.1	26.5	23.2	21.6
	STDev	23.9	20.9	22.5	23.9	20.7	22.9	20.9	20.9	20.9	21.6	21.6	20.9	20.9	18.2	23.8	23.7	23.7	24.5	24.5	24.5
Site 4	MEAN	49.7	43.6	39.2	34.7	58.3	71.4	43.6	43.6	40.2	50.7	50.7	40.2	40.2	44.1	25.3	21.9	20.3	23.9	20.4	18.8
	STDev	32.5	42.9	36.6	30.9	52.4	61.8	42.9	42.9	42.0	45.3	45.3	42.0	42.0	43.9	26.2	24.7	23.9	24.3	22.6	21.9
Site 5	MEAN	23.0	36.0	35.0	33.8	58.6	79.3	36.0	36.0	31.1	47.0	47.0	31.1	31.1	35.6	19.0	13.3	10.5	18.6	12.9	10.2
	STDev	14.6	18.4	17.1	15.6	24.4	30.9	18.4	18.4	17.6	21.7	21.7	17.6	17.6	18.0	12.1	10.8	10.0	11.6	10.3	9.5
Differences between model and data (mg/L)																					
Site 1	MEAN		9.1	9.4	9.7	26.4	42.6	9.1	9.1	4.4	20.4	20.4	4.4	4.4	8.6	-2.0	-6.1	-8.0	-1.9	-6.0	-7.8
	STDev		-0.8	-0.5	-0.3	3.2	9.2	-0.8	-0.8	-1.1	1.1	1.1	-1.1	-1.1	-1.6	-1.4	-1.4	-1.2	-1.3	-1.3	-1.1
Site 2	MEAN		11.9	13.0	14.0	28.1	43.7	11.9	11.9	7.7	21.8	21.8	7.7	7.7	10.3	2.6	-1.5	-3.4	3.1	-1.0	-2.9
	STDev		7.1	8.5	9.6	8.0	10.2	7.1	7.1	7.1	8.7	8.7	7.1	7.1	4.9	8.6	8.1	7.8	9.1	8.7	8.4
Site 3	MEAN		-10.7	-9.4	-8.2	1.4	13.2	-10.7	-10.7	-13.9	-3.6	-3.6	-13.9	-13.9	-13.0	-17.3	-20.7	-22.2	-16.8	-20.1	-21.6
	STDev		-3.0	-1.4	0.0	-3.2	-1.0	-3.0	-3.0	-3.0	-2.3	-2.3	-3.0	-3.0	-5.7	-0.1	-0.2	-0.2	0.6	0.6	0.6
Site 4	MEAN		-6.1	-10.5	-15.0	8.6	21.7	-6.1	-6.1	-9.5	1.0	1.0	-9.5	-9.5	-5.6	-24.4	-27.8	-29.4	-25.8	-29.3	-30.9
	STDev		10.5	4.1	-1.6	19.9	29.4	10.5	10.5	9.5	12.8	12.8	9.5	9.5	11.4	-6.2	-7.8	-8.5	-8.2	-9.8	-10.5
Site 5	MEAN		13.0	12.0	10.8	35.6	56.3	13.0	13.0	8.1	24.0	24.0	8.1	8.1	12.6	-4.1	-9.8	-12.5	-4.4	-10.1	-12.9
	STDev		3.8	2.4	1.0	9.8	16.2	3.8	3.8	2.9	7.1	7.1	2.9	2.9	3.4	-2.5	-3.8	-4.6	-3.0	-4.3	-5.1
Average	MEAN		3.4	2.9	2.2	20.0	35.5	3.4	3.4	-0.6	12.7	12.7	-0.6	-0.6	2.6	-9.0	-13.2	-15.1	-9.2	-13.3	-15.2
	STDev		3.5	2.6	1.7	7.6	12.8	3.5	3.5	3.1	5.5	5.5	3.1	3.1	2.5	-0.3	-1.0	-1.4	-0.6	-1.2	-1.6

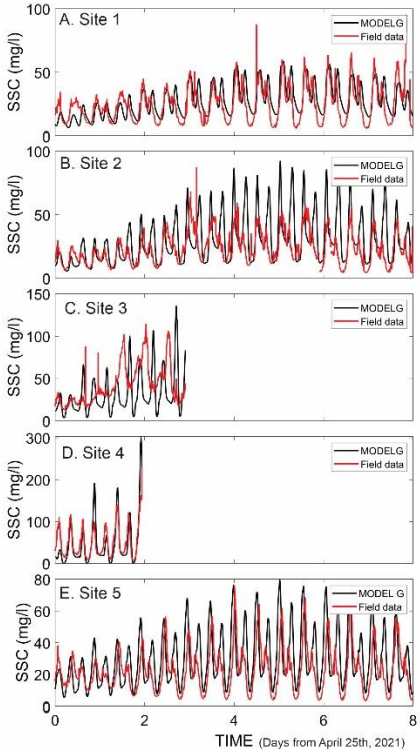

Figure 19: *Comparison between the best model (model G, see Table 3) and the suspended sediment observations, for the period at the beginning of the deployment, when the tide is between neap and spring, and there are no wind waves (the same period used to calculate the statistics presented in Table 3).*

3.7 Calculation of flushing times

Flushing times in Ōhiwa Harbour were calculated by seeding a passive neutrally buoyant conservative tracer, with a concentration of 1 g/m^3 (the initial amount is arbitrary) across all grid cells in the model. Two scenarios were run, one with no river discharge and another with river discharge. The tracer content of water coming at river discharge points and at the open boundary were set to zero. As mixing occurs across the model domain the tracer dilutes and is shown in the flushed out of the cells. The flushing rate is calculated by fitting an exponential curve to the dilution of the tracer for each cell and measuring the time it takes to fall below a threshold concentration of 0.37 in days (E-folding flushing time). A high flushing rate means that the estuary is well-flushed, with a low flushing time.

3.8 Source-sink and harbour tracer analysis

To assess the sediment retention (trapping efficiency and what is lost to open coast) and whether there are any other significant contributions from within the harbour, sediment tracking and tracer analysis were performed. Source sink analysis runs used a constant value of 150 kg/m^3 across all discharge points (streams and cliff erosion points) for sediment tracking throughout the harbour. A high value was assigned to allow a more practical scale for analysing the footprint of sediment throughout the harbour (using observed concentrations resulted in suspended sediment levels that were close to the minimum detectable in the model). The bed characteristics were set to solid, so that there was no resuspension. Note that results are indicative only because the sediment dynamics depend on the total sediment in each sediment. For example, the degree to which sediments settles in one grid cell will depend on the total concentration of sediment in that cell (both new and resuspended), and artificially removing one fraction will also affect how the other fraction behaves. The source-sink analysis was carried out over the entire calibration period (19/4/21 – 17/5/4/21). This sediment was input using the same characteristics as all other runs, and was tracked using the cohesive sediment transport module (so it include sediment settling and re-entrainment from the bed by tidal currents).

To better understand hydrodynamic conductivity in the estuary, passive tracer release experiments from different regions were also conducted by splitting the harbour into nine arbitrary zones based on constriction points and characteristics (Appendix 4, Figure A2). This was conducted as a complement to the cohesive sediment transport modelling used in the source-sink analysis and the scenario modelling. A uniform concentration of 1 gm^{-3} was released across all cells within each individual region separately where all other areas were set to 0 gm^{-3}. To control for the different areas and volumes of the defined sub-regions, tracer was normalised to the initial tracer mass at the time of release by multiplying region area, volume, and tracer concentration. Tracer loss for each region into other areas of the harbour was calculated as the tracer mass at each time step divided by the initial tracer mass. We assumed that no mass returns to the system from outside the ocean boundary (constant input of 0 gm^{-3}). Although this was a neutrally buoyant conservative tracer and does not account for processes such as settling velocities of sediments, it does provide important information on water mass movement and transport from one area of the harbour to another, complimenting further sediment investigations. Results for these investigations are provided in Appendix 4.

3.5 Loading scenarios

Loading scenarios were undertaken for a contemporary current state (based on the year 2014) and climate change altered states. All these scenarios were run for one year, using four 3-monthly blocks.

Firstly, the contemporary state was modelled using wind and river flow forcing from the year 2014, including sediment loads acquired from Manaaki Whenua (Vale et al., 2021). Climate scenarios were done for mid-century (2050) under RCP45 and RCP85. Figure 20 shows the distribution of loading for the whole dataset, compared to the distribution of loading for one year.

Sediments were extracted after a 7-day stabilisation period. Average suspended sediments, and net accumulation rates were calculated for each fraction, and the two mud and two sand fractions were combined to make a total cohesive and total non-cohesive accumulation in each of the 20 by 20 metre grid cells. The morphological adjustment was turned off for all runs (so erosion and accretion occurred, but they were not fed back into the hydrodynamic model). This mainly makes a difference in the dynamic harbour entrance area, where the sand fraction moves around the ebb-tidal delta, and along the open coast boundaries, which can cause instabilities to develop.

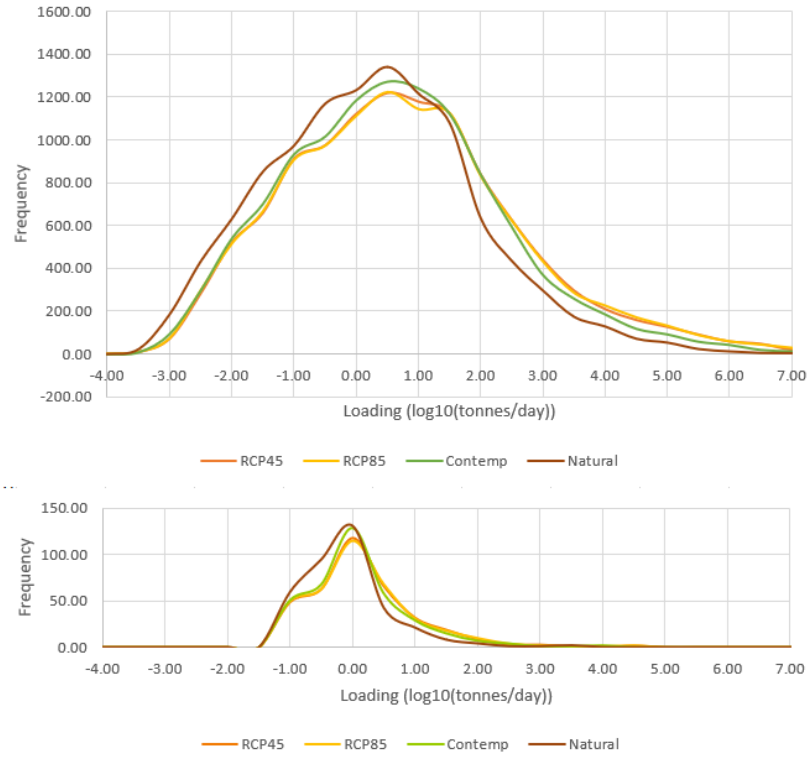

Figure 20: *Top panel: Distribution of sediment loading to the Harbour for all years 1990-2020. Bottom panel: Distribution of sediment loading for 2014 reference year.*

In addition, the accumulation of mud was summed across the domain to compare different areas of the Harbour (these areas are shown in Figure 21). These were also summed at each depth increment, so that, for example, sub and intertidal deposition could be compared.

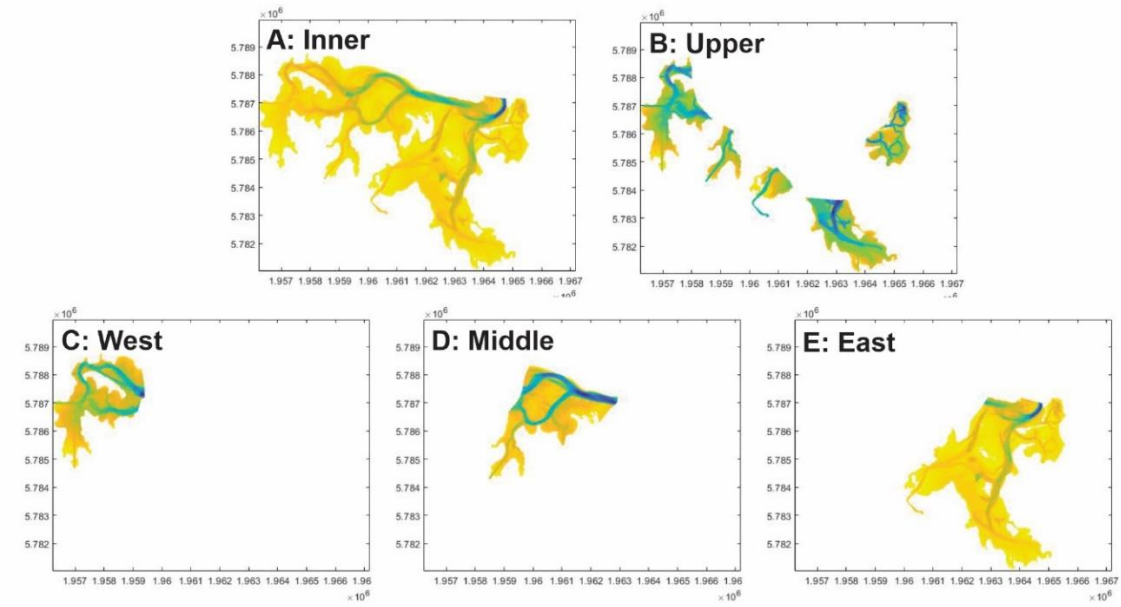

Figure 21: *Showing the areas within the harbour where mud accumulation rates were summed for each scenario, to allow a detailed comparison.*

4. RESULTS

4.1 Spatial variations

Hydrodynamic model results show that tidal currents are strong in channels and much weaker in intertidal areas (Figure 22a). Residual circulation patterns show that around the entrance, flooding and ebbing currents can take different pathways, creating eddies around the flood and ebb tidal deltas (as is common in all barrier-enclosed estuaries). The Nukuhao Stream channel is ebb dominant, and the flow converges into the channel draining the western arbour, which is also ebb-dominant. The main channel into the harbour is flood dominant, which combined with the western channel, form a clockwise eddy. In contrast to the western channel, the eastern channel is nearly always flood dominant. The tidal currents also control the flushing time of the harbour (Figure 23), and there are strong spatial variations in the flushing tide, with the western part of the harbour having flushing times that are 8-10 days. Conversely the eastern channels and the Nukuhou Stream channel has a flushing time of 1-3 days. The very long flushing time of the western channels is because of all the islands and constricted channels, and also because the main entrance has migrated to its most easterly position. Presumably, at some point in the geological past, the spit may have breached, in which case western flushing would have been much more effective. This poorly flushed region corresponds to the area of muddy channels shown in Figure 3.

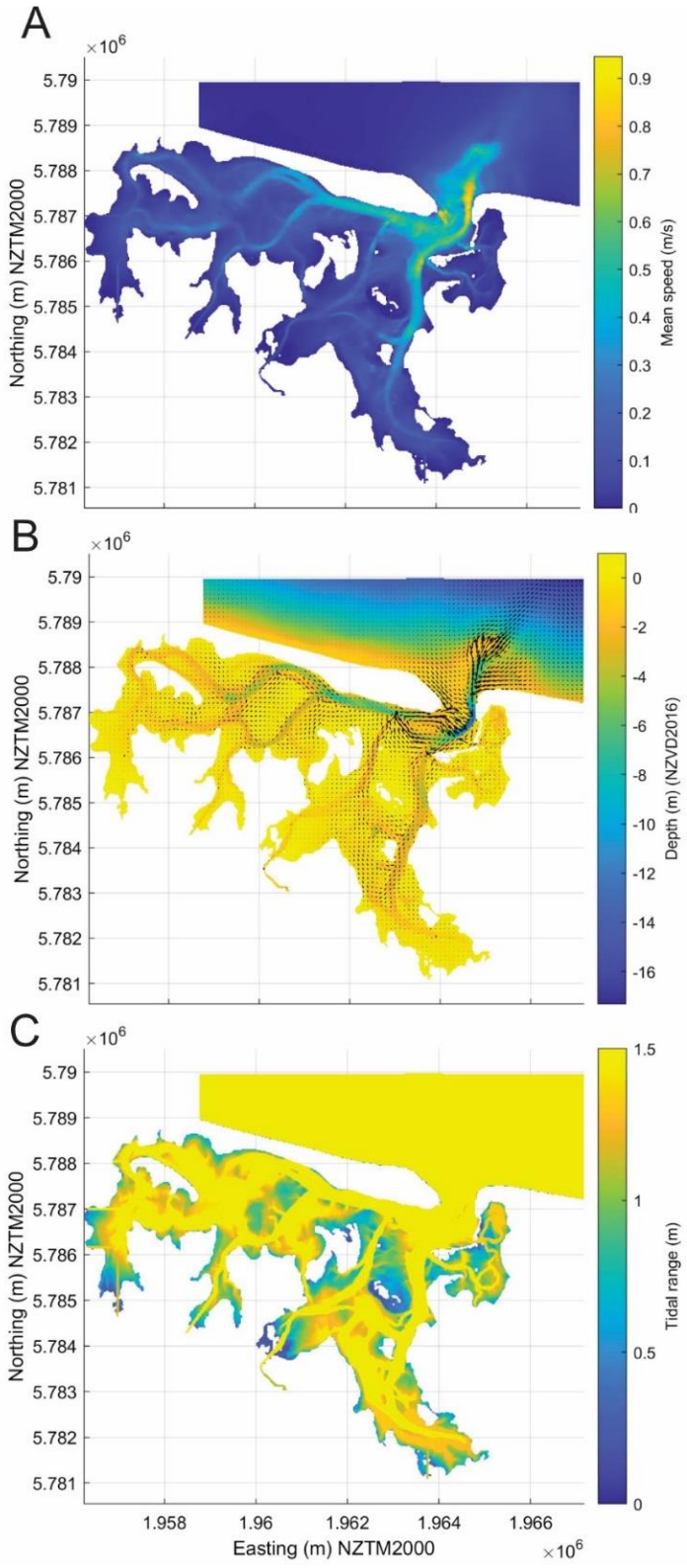

Figure 22: *Modelled hydrodynamic conditions during the calibration period. A: The mean speed calculated at each model grid cell. B: The residual current vectors plotted on top of the bathymetry. A larger version of this panel is provided in Appendix 3 C: The tidal range (the elevation of high tide minus the elevation of the lowest low tide at each grid cell in the model). This is equivalent to the maximum inundation depth in intertidal regions. Land areas in all panels are plotted white.*

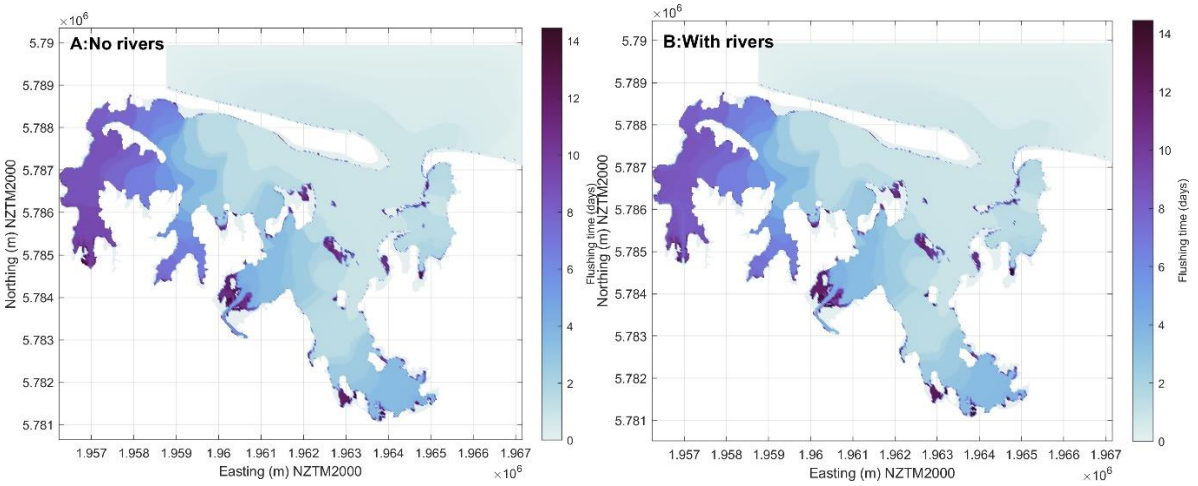

Figure 23: *Flushing time at each grid cell. Flushing time is calculated as the inverse of the decay rate of tracer seeded in the model at each grid cell prior to running the model for the calibration period. A: Without including river and stream discharge. B: Including river and stream discharge (the main difference is a reduction of the flushing time (~ 2 days) in the western sub-estuary (near the Burma, Waiotane and Wainui streams, Figure 1).*

Suspended sediment characteristics (Figure 24) reflect the strength of tidal currents, and so are greater in harbour channels. Sand is mostly suspended around the harbour entrance because it is only in this region that currents are above the entrainment threshold for sand. Although the currents are strong enough to entrain mud in the entrance region, there is no mud there to entrain, and so the only mud in the model has been advected by the tidal currents from areas landward (ebbing currents) and seaward (flooding currents) of each grid cell. The model was very sensitive to where the mud was placed. More mud in the landward part of the domain makes the sediment transport ebb-dominant, and more seaward makes the sediment transport more flood-dominant. The abrupt and unnatural boundary in the model between the areas with mud and the areas with no mud caused unnatural patterns in the erosion-accretion (net accumulation) of sediment in channels. These have been masked from Figure 26c. Sand eroded and accreted around the dynamic entrance area with no net pattern, and mud accumulated on the intertidal flats.

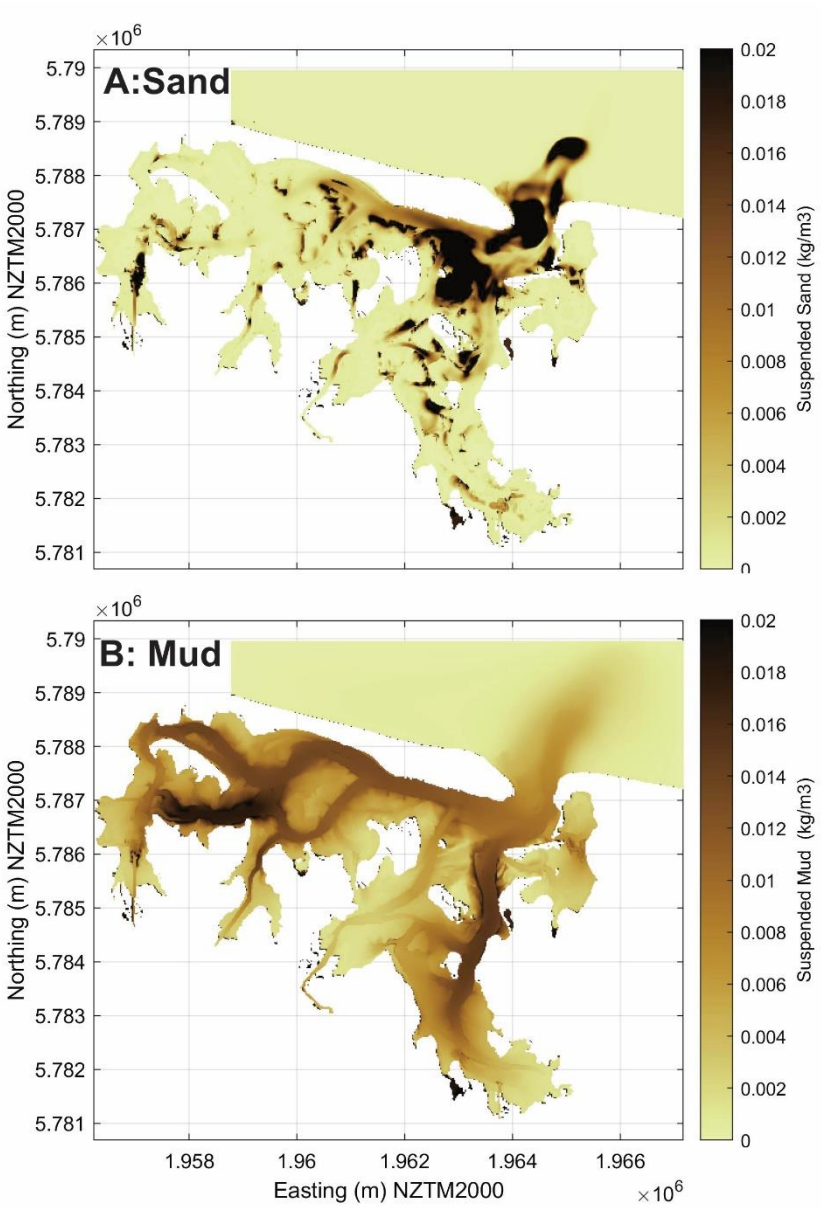

Figure 24: *Average suspended sediment concentration over the calibration period, using the best model G (see Table 2). The sand fraction includes both the coarse and fine sand fractions, and the mud fraction includes both mud fractions (see the initial distribution in Figure 16).*

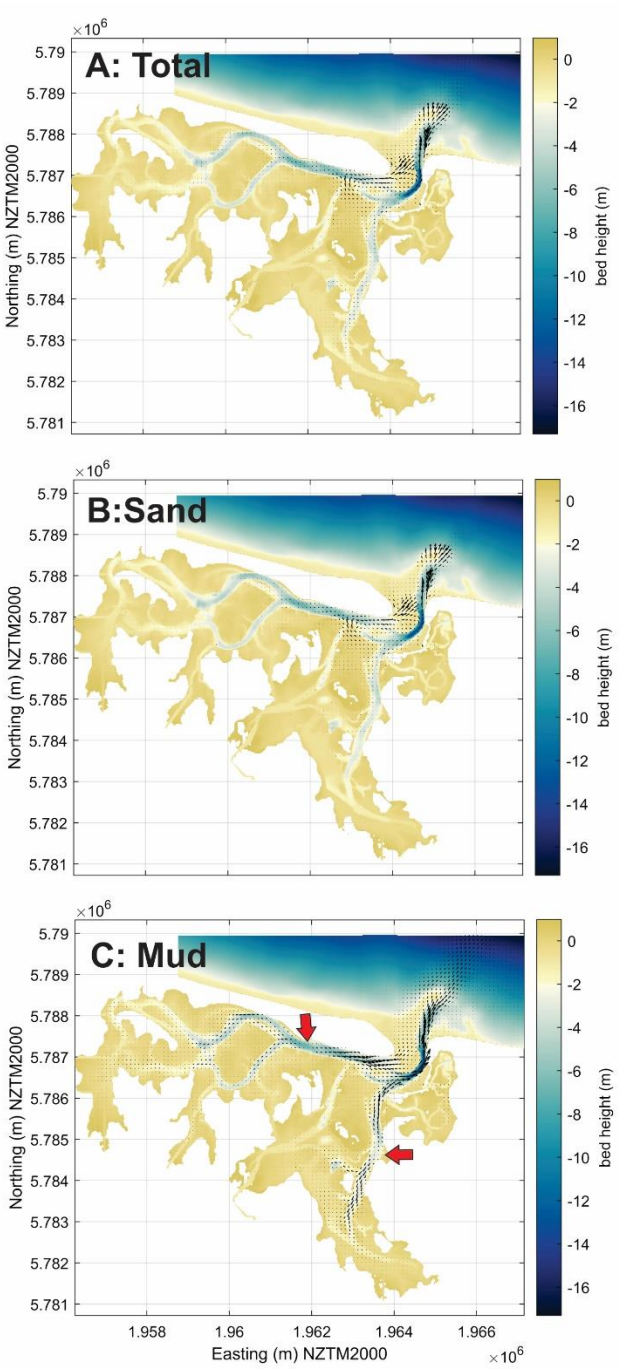

Figure 25: *Maps of average suspended sediment flux (the length of arrows show the relative size of the flux, and the orientation show the direction of the flux). A larger version of panel C is provided in Appendix 3. The red arrows on the bottom panel show the point where the flux transitions from net importing to net exporting. The background colour shows the bathymetry. Model runs are for the calibrations time period using Model G from Table 2.*

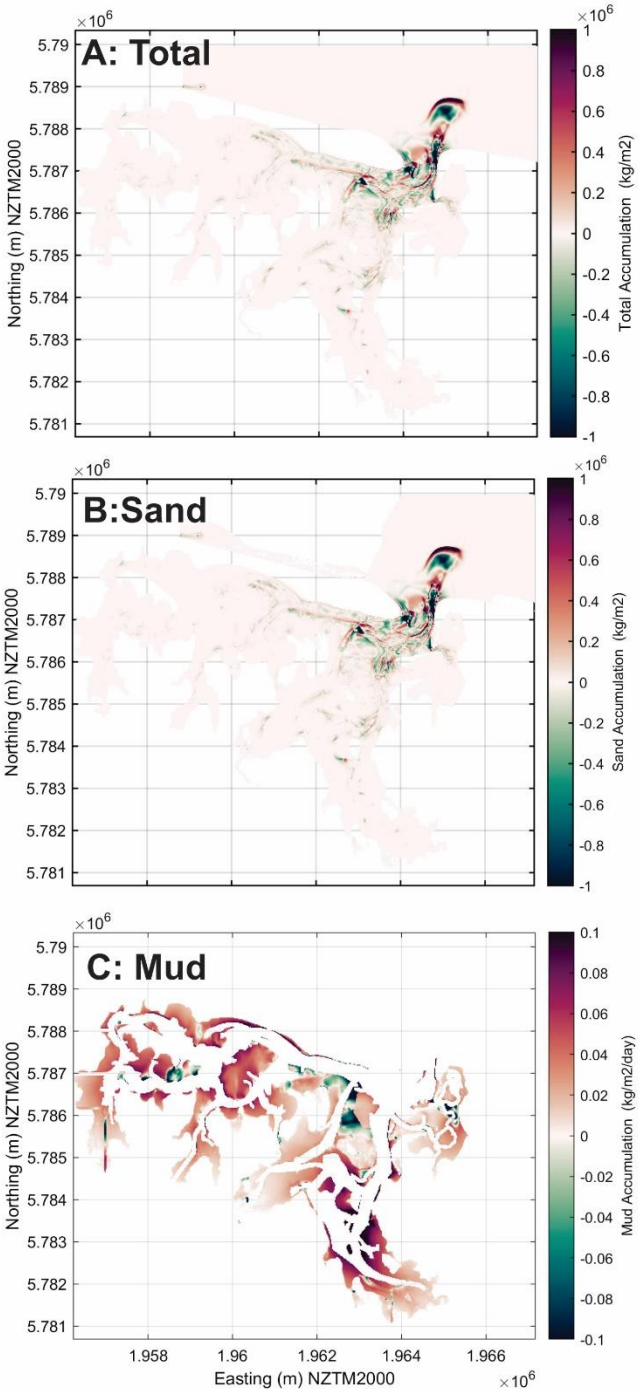

Figure 26: *Spatial distribution of sediment accumulation or erosion, relative to the initial bed stores, for the 2014 calibration run (the duration of the deployment period). Initial bed stores are calculated after a spin up time of 13 tidal cycles (about 7 days). Note that in panel C, erosion/accretion in channels and offshore is not shown. This is because some of the channel areas had no mud in the initial set up (Figure 16 shows the initial distribution of bed texture), and so mud cannot be eroded in these areas.*

4.1 Sediment loading scenarios

In this Section, we present the results of the sediment loading scenarios. The changes to loading were run with 2014 as the baseline hydrodynamic conditions, and each with a total duration of year. The differences in suspended sediment and accumulation were plotted for each of these scenarios relative

to the ‘Natural’ conditions, as difference maps. The differences between scenarios are small, and it is difficult to see the differences clearly. The differences are small because the climatic conditions are the same for every run, the only differences are the loading conditions, and loading was generally very small. To better highlight the differences, we have also summed the cohesive fractions as a function of depth, sub-divided into different regions of the harbour. These areas are shown in Figure 21 and summarised in Table 4 (for the cohesive sediment fractions).

Prior to interpreting the difference plots, it is useful to provide a clearer understanding of the summed data and Figure 27 shows the distribution of these values for the ‘Natural’ scenario. Suspended sediment increases generally with depth, and when summed across the grid, is greater in the deeper channels. This is because the currents are generally higher in channels, which retains finer sediment in suspension. Also finer sediments are advected over long distances, from intertidal areas into channels. Sediments settle where the currents are lowest, so tend to settle in the intertidal regions and get eroded from channels. Figure 27c and d shows erosion in deeper areas and accumulation in intertidal regions, which is particularly evident when accumulations is summed over these regions (d). In the deep part of the grid offshore (not shown in the Figure), sediment eroded from the estuary is deposited offshore, and advected out of the model at the open boundaries. Figure 27 also shows that sediment tends to accumulate in upper reaches of the harbour. Note that there is very little of the active model grid above 1m relative to MSL (the far-right panel shows the number of grid cells with this elevation in the model), and so there is little accumulation here.

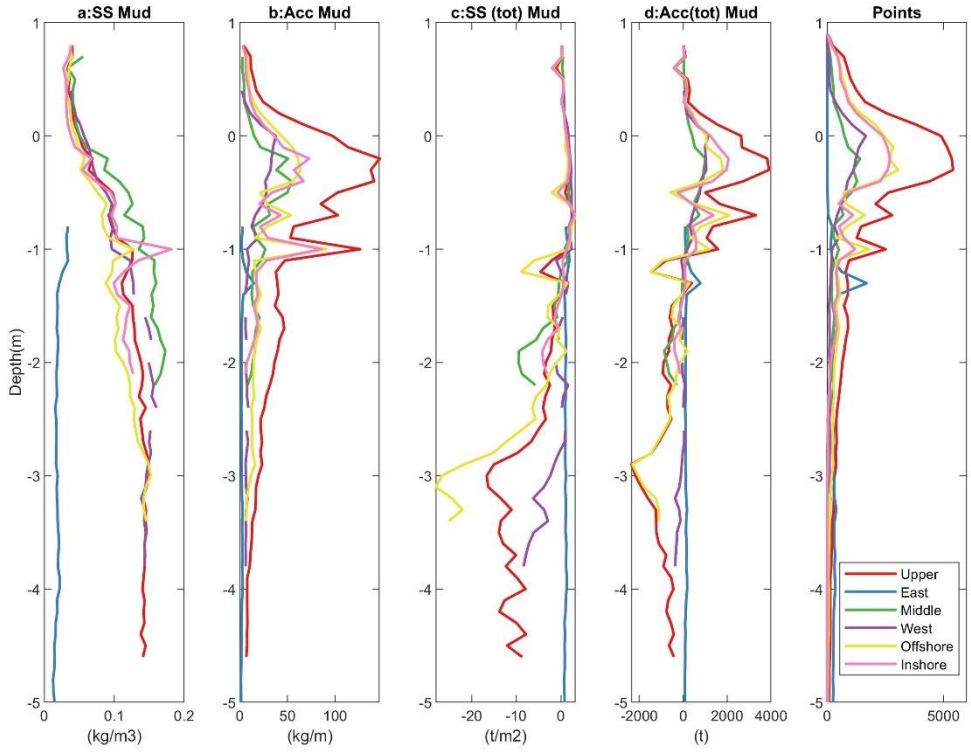

Figure 27: *Output from the year-long Natural loading condition model, for the two cohesive fractions only (added together). a) Average suspended sediment concentration at each grid cell. b) Average accumulation at each grid cell. c) Total suspended sediment concentration over each subregion of the grid. d) Total*

accumulation over each subregion of the grid. The far right panel indicates the number of grid cells at each elevation.

Figures 28-31 show the difference maps between scenarios, where the differences have been averaged for year. Suspended mud tends to be higher in the channels compared to the Natural state, and also accumulates in the channel and high intertidal areas. Sand is not discharged into the model by the rivers, so all changes occurring in the model are caused by sand remobilising from the bed and moving around the channels. Since the hydrodynamics are identical between runs, differences are close to the resolution of the model and are due to small instabilities, and the effect of mud on sand resuspension. In general, the differences between scenarios are not great enough to be highlight well with these difference maps.

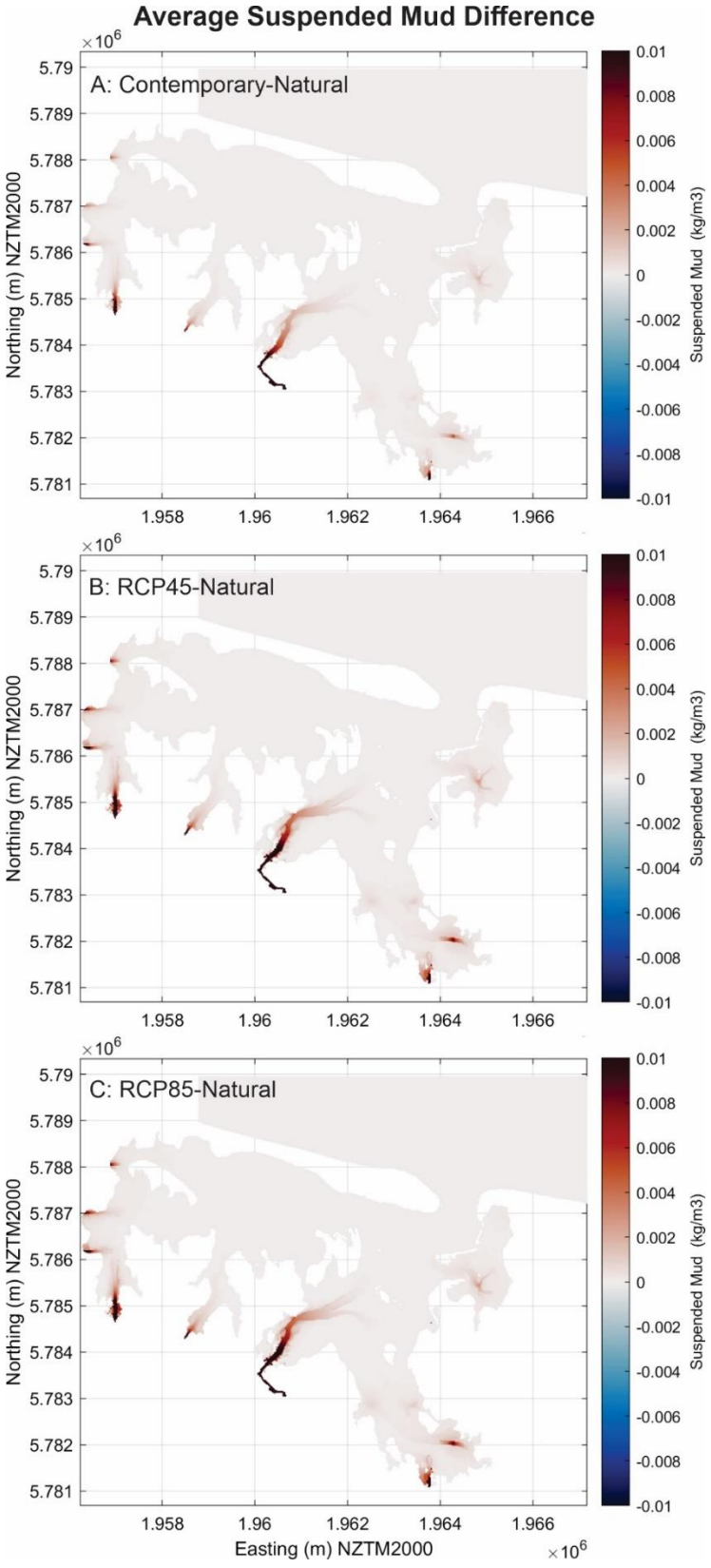

Figure 28: *Comparison of suspended mud differences between all scenarios (relative to the Natural scenario). Results are run with the 2014 hydrodynamic conditions for a year and averaged. Blue (negative) means that Natural scenario is greater.*

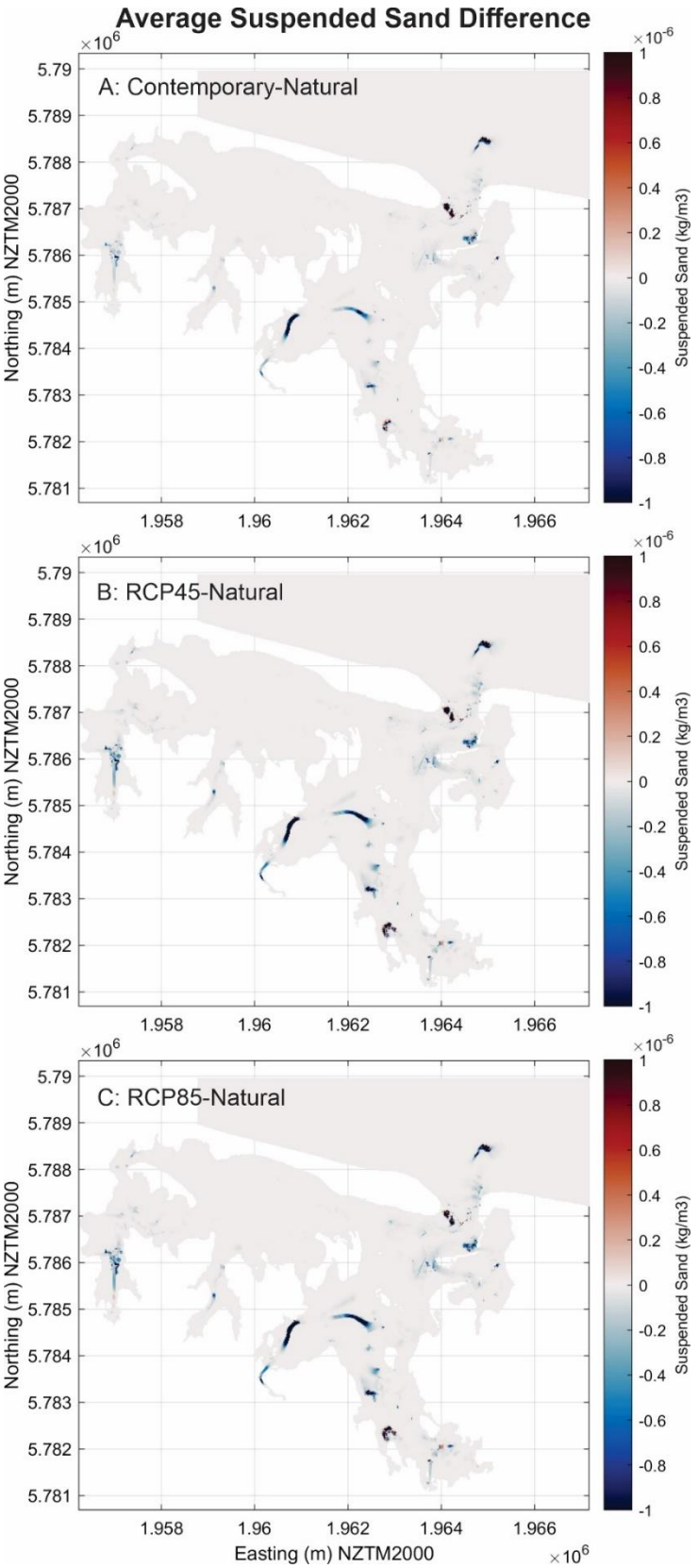

Figure 29: *Comparison of suspended sand differences between all scenarios (relative to the Natural scenario). Results are run with the 2014 hydrodynamic conditions for a year and averaged. Blue (negative) means that Natural scenario is greater. Note that the changes are very small scale compared to the mud changes, and are likely below the resolution of the model.*

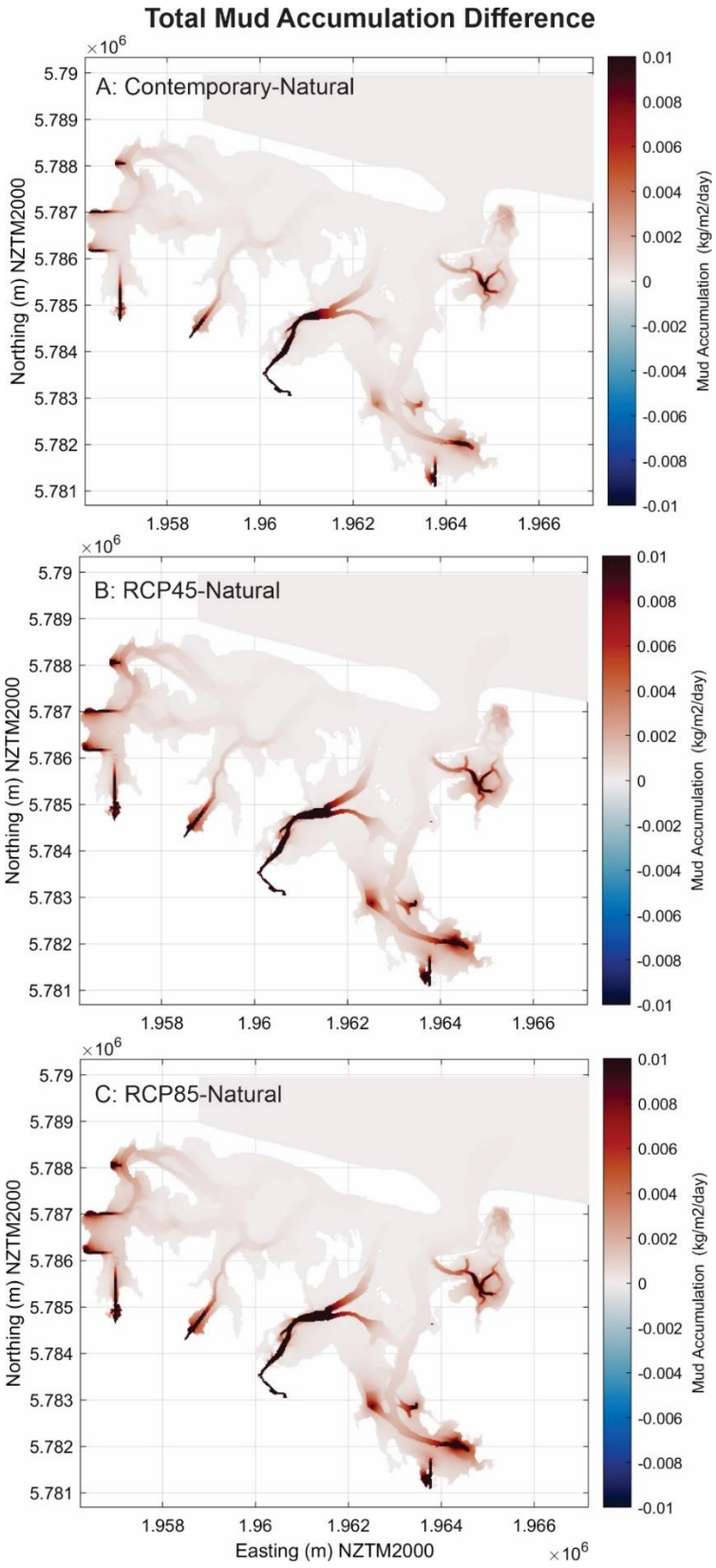

Figure 30: *Comparison of accumulated mud differences between all scenarios (relative to the Natural scenario). Results are run with the 2014 hydrodynamic conditions for a year and averaged. Blue (negative) means that Natural scenario is greater.*

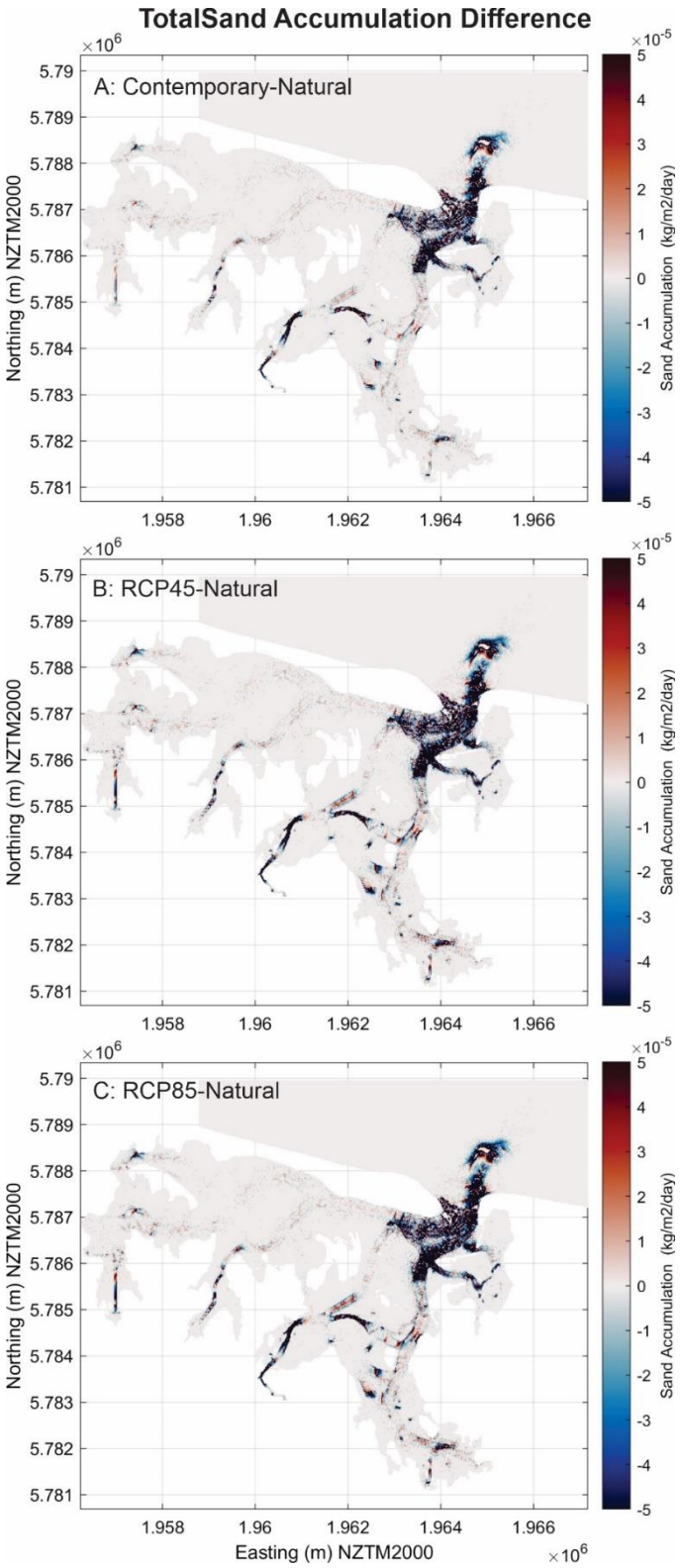

Figure 31: *Comparison of accumulated sand differences between all scenarios (relative to the Natural scenario). Results are run with the 2014 hydrodynamic conditions for a year and averaged. Blue (negative) means that Natural scenario is greater. Note that the changes are very small scale compared to the mud changes, and are likely below the resolution of the model (and the reason they are noisy).*

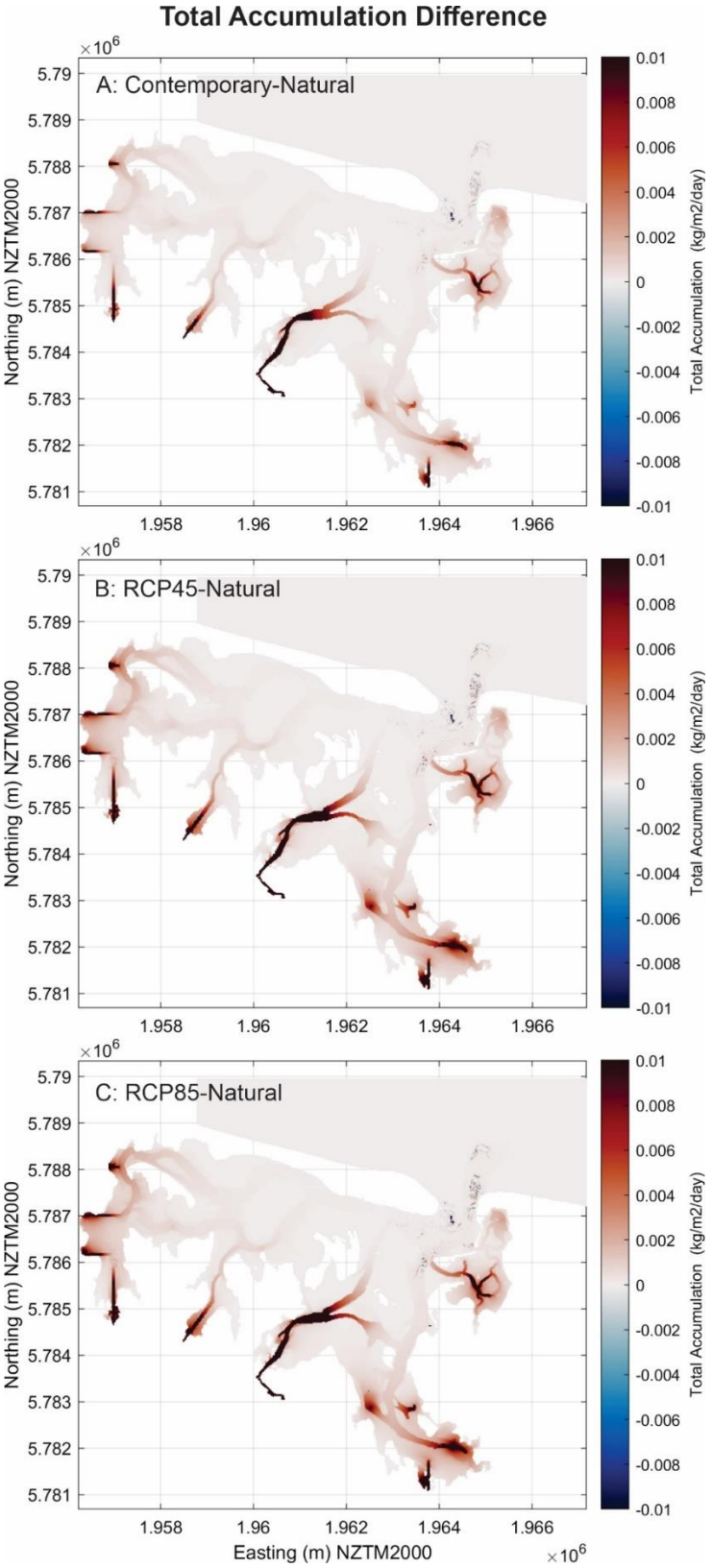

Figure 32: *Comparison of sediment accumulation (sand and mud) differences between all scenarios (relative to the Natural scenario). Results are run with the 2014 hydrodynamic conditions for a year and averaged. Blue (negative) means that Natural scenario is greater.*

In general, mud suspension and accumulation was more affected by changes to hydrodynamic conditions than loading changes, except when the loading occurred in an extreme event. This is shown in Figure 33, where we have summed the accumulation that occurred in each area of the harbour over a week. Accumulation and suspended sediment timeseries in each grid cell varies strongly over a tidal cycles (as shown in the calibration dataset and in Figure 17), and so care was taken to sum integral tidal periods. Sediment varied a lot with weekly changes to the tidal range and wind conditions over the year, and these were more a driver of accumulation patterns then changes to the freshwater loading into the estuary. In Figure 33 (right panels), the accumulation rates have been normalised by the tidal variations on the outer boundary, in order to control for the tidal variations in the accumulation rates. It is only the very large event (which is well beyond the normal distribution of events for the whole loading dataset, plotted as lines in the left panel), that shows a substantial harbour response.

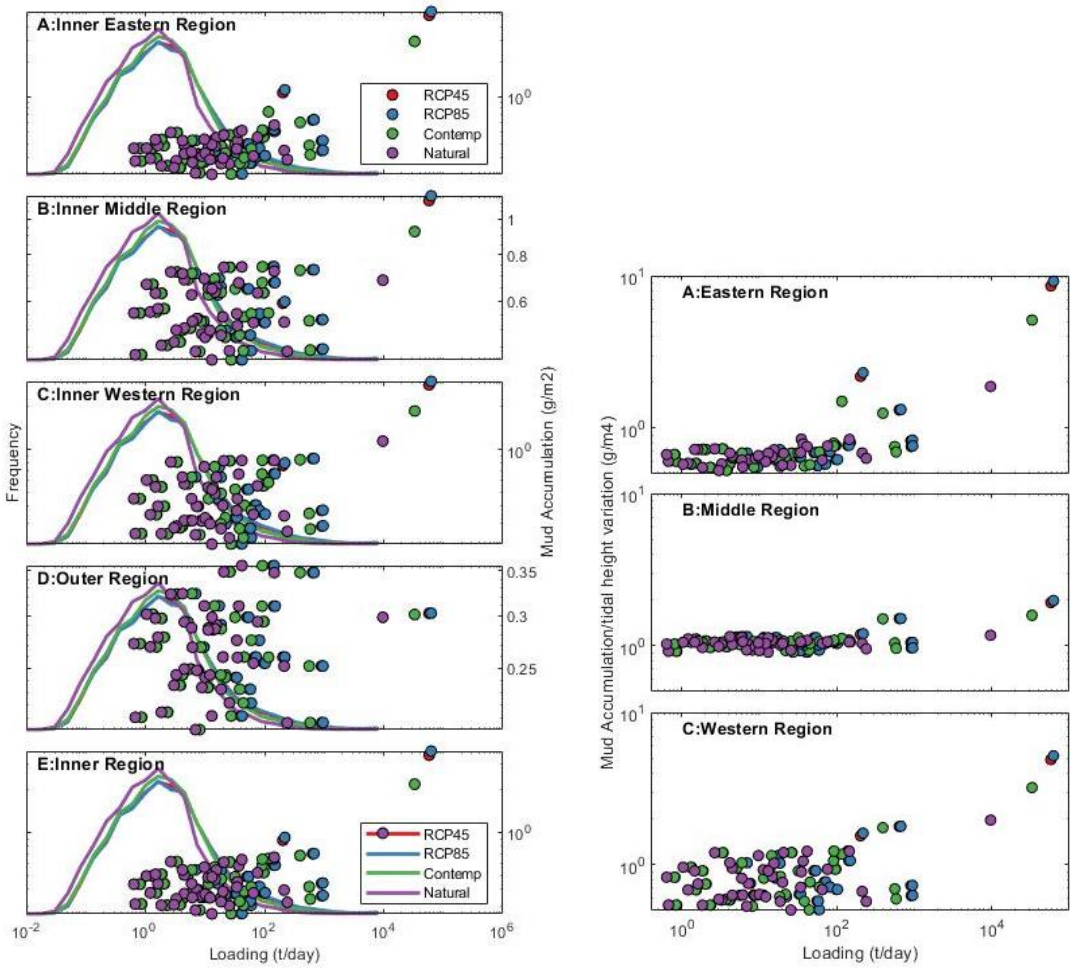

Figure 33: *In these panels, the weekly-averaged mud accumulation for each region, and for each scenario, plotted as a function of the average loading for that same week (so each scenario provides 52 points). In the right panel, the mud accumulation has been normalised by the variation of tidal height at the outer boundary for that week, as much of the variation in accumulation in the Harbour is because of spring-neap variations to resuspension/accretion within the harbour. The background lines in the left panel represent the daily distribution of the whole (20-year) loading dataset.*

The channel draining the intertidal mud flats in the upper region of the harbour trap much of the new sediment delivered into the model, and these differences increase between natural, contemporary, RCP45 and RCP85, with the biggest difference natural and contemporary, and between contemporary and the two RCP scenarios (which are quite similar). The greatest difference is in the western part of the grid, where more sediment is trapped on the high intertidal.

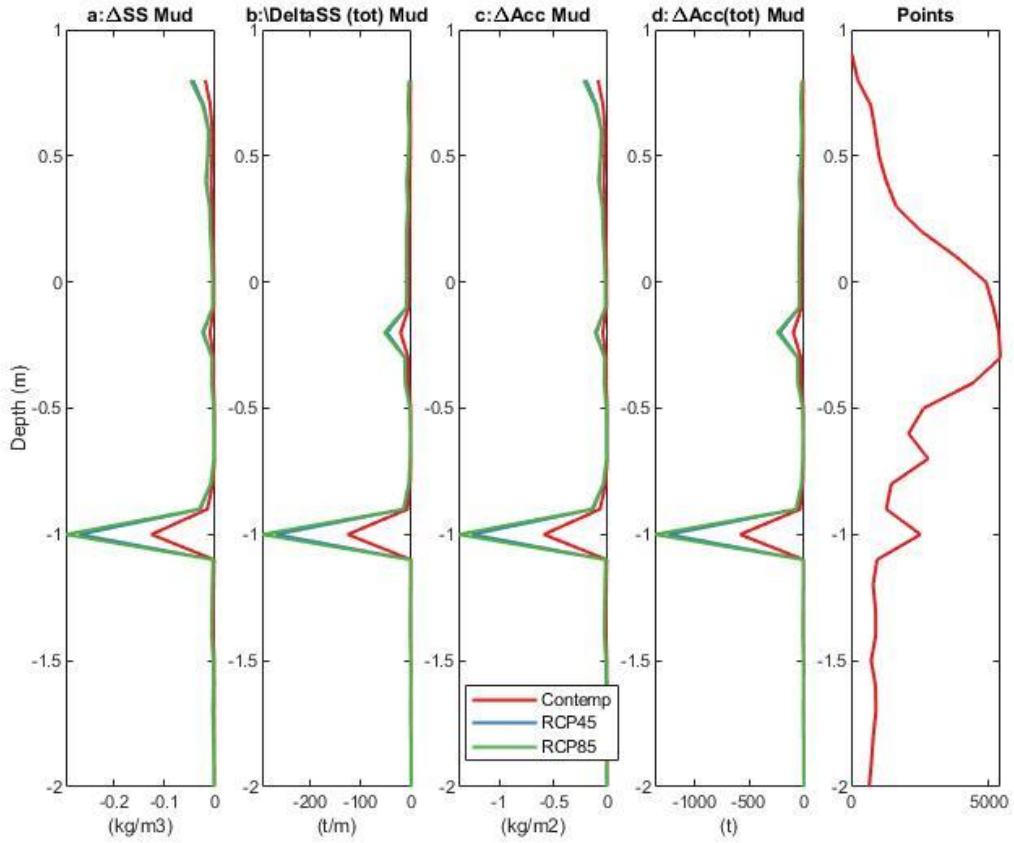

Figure 34: *Relative difference in average suspended mud (a); total suspended mud (c) average accumulated mud (d) total accumulated mud for the inner region of the grid.*

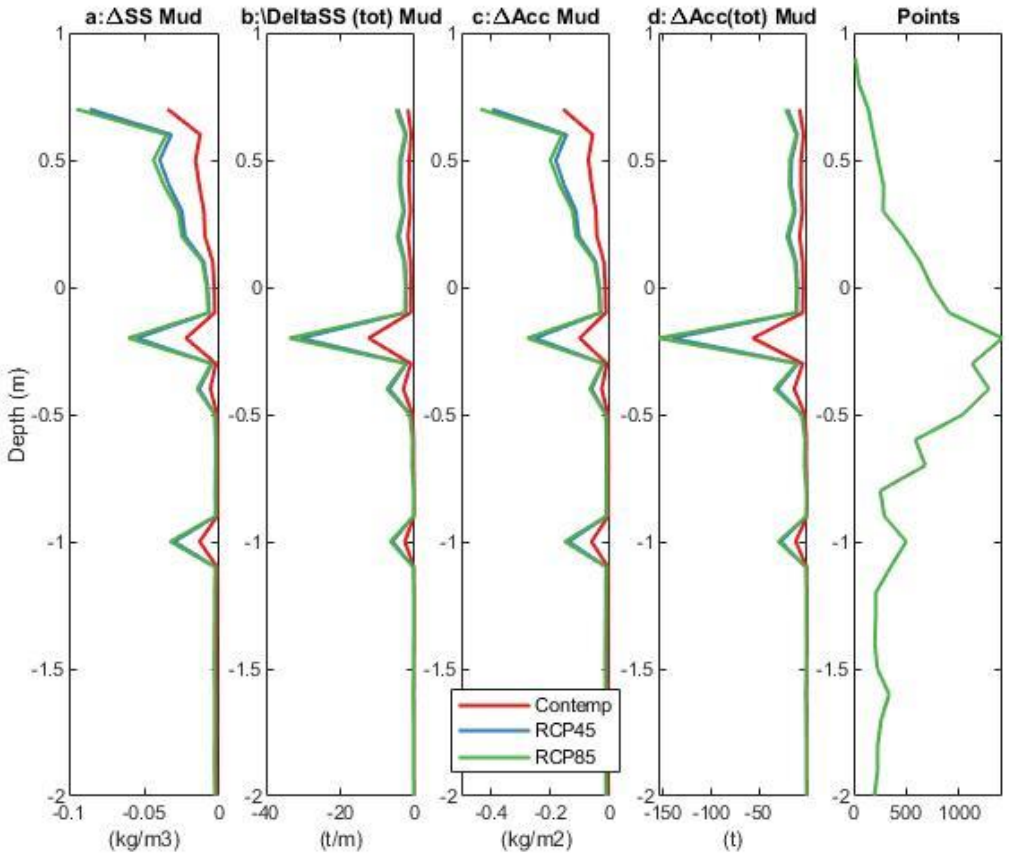

Figure 35: *Relative difference in average suspended mud (a); total suspended mud (c) average accumulated mud (d) total accumulated mud for the western region of the grid.*

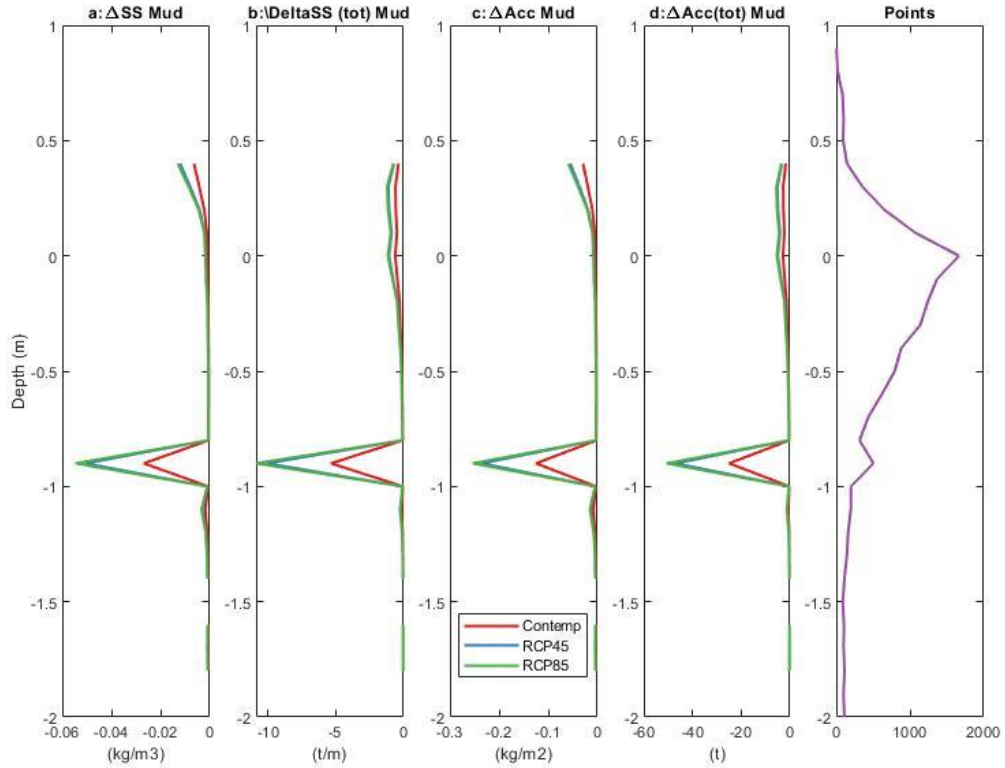

Figure 36: *Relative difference in average suspended mud (a); total suspended mud (c) average accumulated mud (d) total accumulated mud for the middle region of the grid.*

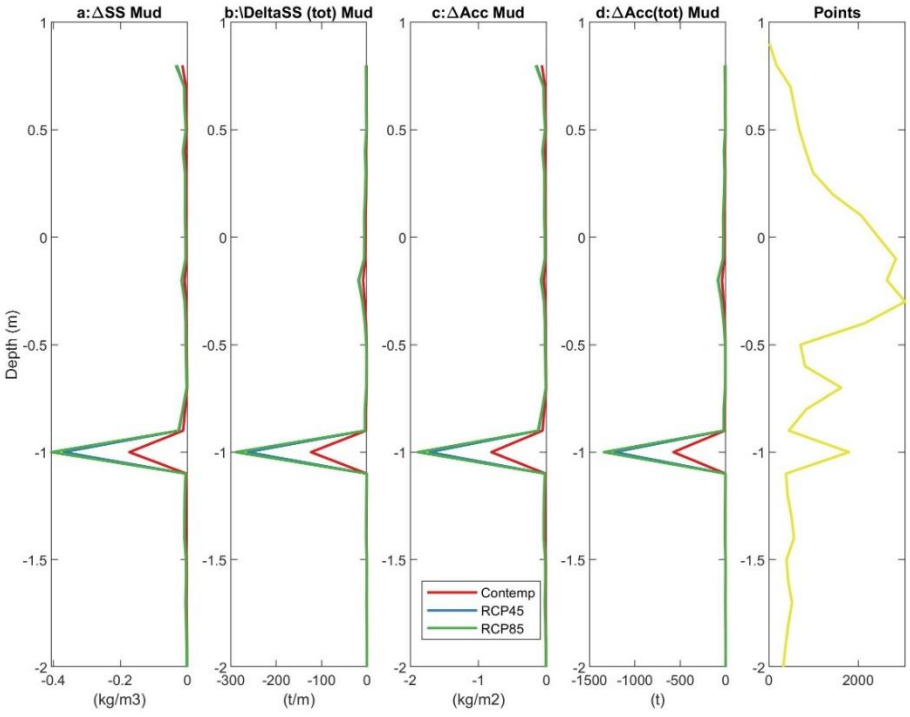

Figure 37: *Relative difference in average suspended mud (a); total suspended mud (c) average accumulated mud (d) total accumulated mud for the eastern region of the grid.*

As a final comparison between scenarios, the total accumulation rates were summed in each of the areas (shown in Figure 21), and also in the intertidal areas (for latter mud only) and the results are provided in Table 4. This was to see what percentage of the sediment loading in the model was trapped within the model domain, and what fraction was lost to the open ocean. Unfortunately, in all cases, the model consistently lost sediment to the open ocean despite new sediment being introduced at discharge points. The model was therefore not in equilibrium prior (even though there was a long warm up period). Prior studies show that it can take many years for the model to approach equilibrium, and the equilibrium depends strongly on the number of grainsizes used and their spatial distribution in the initial set up. Although we undertook extensive calibration, it clearly did not lead to an equilibrium model, and this is a limitation of the study.

To control for natural losses of sediment from the domain, the accumulation rates were linearly extrapolated to determine the likely accumulation at zero loading (the ‘none’ row in Table 4). This accumulation rate was then removed from the total accumulation in each loading scenario (“corrected for natural loss”. It is then possible to conclude that the accumulation in contemporary times is 3 times that of the natural state, and this could increase to 5.5 and 6 times under RCP45 and RCP85 respectively. Even with this correction, only a small fraction is retained in the model domain. At the moment, the concentration at the open ocean boundary is set to zero. In reality, the sediment lost at the outer boundary might be brought back into the model with a change in the tide. The improve this, the model would need to be nested within a much larger grid (which would also increase the computation time).

.

Table 4:*The total mud and sand accumulated in each region of the model grid (shown in Figure 21). The intertidal areas (>-0.8m) is represented separately, which is above the depth of the channels that show strong mud accumulation. The rows marked 'none' represent the linear extrapolation of trapping over all the runs, plotted as a function of loading. This is was done as an attempt to correct for the loss of sediment from the domain that occurs with natural conditions and no loading (the domain is not in equilibrium and looses sediment to the open ocean).*

	Actual						**Difference**						**Input load**	**Actual**			
	Inshore	**Offshore**	**West**	**Middle**	**East**	**Upper**	**Inshore**	**Offshore**	**West**	**Middle**	**East**	**Upper**		**Total Domain**	**Corrected for natural loss**	**Inner Domain Corrected**	**Upper Domain Corrected**
MUD	kt/yr												kt/yr				
Natural	-14.5	11.3	3.3	-6.6	-13.7	10.2	Postive(red) means natural smaller						11	-3.22	0.47	0.47	0.45
Contemp	-13.5	11.3	3.4	-6.5	-12.9	11.2	1.00	0.00	0.16	0.05	0.79	0.95	36	-2.21	1.47	1.47	1.40
RCP45	-12.4	11.3	3.6	-6.5	-12.0	12.2	2.11	0.00	0.38	0.09	1.64	2.01	62	-1.10	2.58	2.58	2.46
RCP85	-12.2	11.3	3.7	-6.5	-11.9	12.4	2.31	0.00	0.42	0.10	1.80	2.20	67	-0.90	2.78	2.78	2.65
None	-15.0	11.3				9.8							0	-3.68			
Intertidal MUD																	
Natural	24.5	0.1	6.4	7.7	9.7	10.6	Postive(red) means natural smaller						11	24.59	0.16	0.16	0.15
Contemp	24.9	0.1	6.5	7.7	9.9	10.9	0.33	0.00	0.14	0.02	0.17	0.31	36	24.91	0.48	0.48	0.46
RCP45	25.2	0.1	6.7	7.7	10.1	11.3	0.70	0.00	0.33	0.03	0.33	0.66	62	25.28	0.85	0.85	0.81
RCP85	25.3	0.1	6.7	7.7	10.1	11.3	0.76	0.00	0.37	0.04	0.36	0.73	67	25.35	0.92	0.92	0.88
None	24.4					10.5							0	24.43			
SAND	kt/yr																
Natural	-0.8	-7.7	-0.5	13.1	-65.6	-7.6	Note difference are very small						0	-8.45	-8.45		
Contemp	-0.8	-7.7	-0.5	13.1	-65.6	-7.6	0.00	0.00	0.00	0.00	0.00	0.00	0	-8.45	-8.45		
RCP45	-0.8	-7.7	-0.5	13.1	-65.6	-7.6	0.01	0.00	0.00	0.00	0.00	0.00	0	-8.44	-8.44		
RCP85	-0.8	-7.7	-0.5	13.1	-65.6	-7.6	0.01	0.00	0.00	0.00	0.00	0.00	0	-8.44	-8.44		

Finally, Figure 38 shows the source-sink analysis (the passive tracer analysis is shown in Appendix 4). This shows the area of influence of each freshwater discharge or "cliff" discharge point. Note that the scale of accumulation is several orders of magnitude smaller than those shown with the models that included resuspension (even though the loading was increased dramatically for these scenarios).

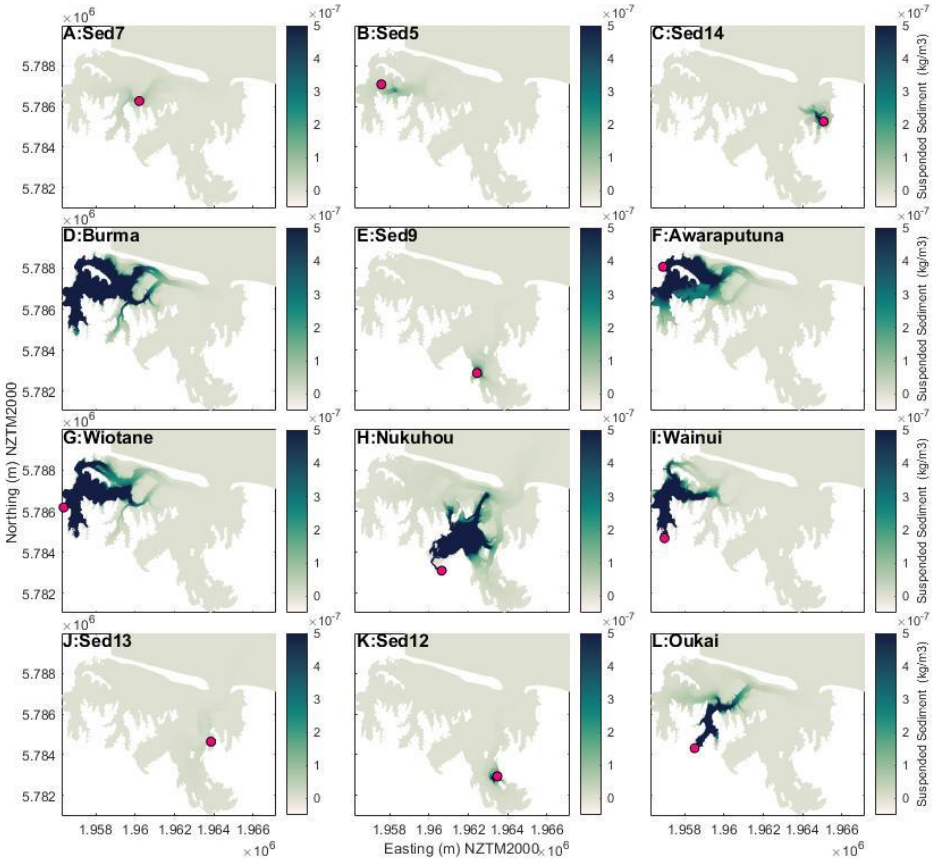

Figure 38: *The average suspended sediment concentration over the calibration time (Model G in Table 2) from sediment arising from the river and stream discharge only. The bed resuspension has been turned off in these runs. Although the scales are the same, note that they are much lower than the sediment concentrations show in Figure 24**:** Average suspended sediment concentration over the calibration period, using the best model G (see Table 2). The sand fraction includes both the coarse and fine sand fractions, and the mud fraction includes both mud fractions (see the initial distribution in Figure 16). The location of discharge points is given in Figure 1, and marked with a magenta circle in each panel.*

5. SUMMARY AND CONCLUSIONS

A hydrodynamic modelling study was undertaken to better understand sediment exchange within Ōhiwa Harbour, and to assess sediment transport and accumulation under different loading and climate change scenarios.

- Modelling demonstrated the complex patterns of advection associated with the tide and how different types of sediment are suspended and transported with incoming tides (fine sands) and with outgoing tides (muds and silts).
- Strengths of the study were the continuous high-resolution SSC (mg/L) field measurements to calibrate and assess sediment dynamics. It is not common among other modelling sediment

studies at this scale to determine whether realistic suspended sediment transport patterns are predicted.

- Stream and river input of sediment into the harbour over the simulation periods were small and did not drive changes in SSC (mg/L) significantly. However, increases in sediment loading between scenarios caused increase in accumulation within the model domain (there was a linear relationship).
- A limitation of the study is that extreme flows were not modelled, especially for the climate change scenarios. It is likely that rainfall patterns and wind will become more extreme by mid-century but the sediment loading in models used hydro-meteorological conditions from 2014.
- The 2014 year contains a usually large event. Weekly analysis shows that this particular event could make a significant change to accumulation rates throughout the domain. This suggests that legacy sediment loads delivered by one-off extreme event may be reworked over time to be deposited around the harbour with the tide and internal processes.
- Sensitivity tests showed importance of internal parameters on sediment dynamics in the harbour, such as the settling rate, erosion rate and critical erosion threshold, and most importantly, the initial distribution of sediments in the domain.
- Waves and resuspension could also add to trapping and resuspension. This was not modelled because of the difficulty of setting a whole new suite of parameters associated with wave mobilization.
- Maps show sand accumulation and dynamics around the harbour entrance and mud accumulation in the middle tidal flats and upper regions. Accumulation in the harbour could double with climate change, and be up 5.5 or 6 times greater than natural levels. Accumulation is particularly concentrated in the upper reaches of the estuary (far from the entrance).
- Flushing times show that the upper region is a sink region with longer flushing times whereas the southern region of the harbour is well flushed with the ocean. The areas dominated by mud content have long flushing times and areas that are sandier have more rapid flushing times.
- Sediment tracking from streams and a minor component of “cliff” erosion showed the distribution throughout the harbour. “Cliff” erosion was used to simulate the combined effect of small catchments with no clear freshwater discharge into the model.
- Tracer experiments demonstrated water mass movement between different harbour regions and showed which regions exchange more with ocean. Water from the Nukuhou River region, for example, ends up in the southern muddy sub-estuary area or the middle part of the harbour.
- Accumulation rates in upper regions and erosion at the harbour entrance – modelling shows how tides scour the channels and deposit sediment in intertidal flat regions.
- A limitation with the modelling is the timescales and resolution – it is difficult to model and capture years of continuous data to understand the accumulation responses to dynamic events and longer timescale process.
- In terms of management, it is clear that the upper southern regions are zones where any input of muddy sediment from the land will accumulate and settle due to higher residence times.

6. ACKNOWLEDGEMENTS

This research was funded by Bay of Plenty Regional Council. Professor Kura Paul-Burke (Ngāti Awa) provided expert local advice on Harbour dynamics and assisted with planning and appropriate placing of moorings. We thank Chris Morcom, Andrew La Croix, Rex Fairweather, Joe Butterworth, and the boat skipper for their help in deploying instruments. Zhanchao Shao provided Sentinel-2 satellite imagery.

7. REFERENCES

Beetham RD 2012. Ohope Beach landslide of 18 June 2011. GNS Science Report 2011/46.

BOPRC 2014. Ōhiwa Harbour Strategy Strategic Policy Publication 2015/02. Retrieved from https://cdn.boprc.govt.nz/media/610368/ohiwa-harbour-strategy-refreshed-2014- final-web.pdf

BOPRC 2015. Bay of Plenty Regional Freshwater Management Framework 2015 Retrieved from https://cdn.boprc.govt.nz/media/445979/bay-of-plenty-regional-freshwatermanagement-framework-2015-web.pdf

Bulmer, R. Research Scientist - National institute of water and atmosphere (NIWA), New Zealand, 'Personal Communication' - 2022.

Bruce, D., 2023, Sedimentation and geochemistry of Ōhiwa Harbour, New Zealand, unpublished M.Sc. (Research) thesis, Earth and Environmental Sciences, University of Waikato, 102 pp.

Chappell, P.R., 2013. The climate and weather of the Bay of Plenty, National institute of water and atmosphere (NIWA), New Zealand, 3rd edition.

Collins, D., Semadeni-Davies, A., 2015. Water resource impacts of forest pasture conversion in the Ohiwa Harbour catchment, National institute of water and atmosphere (NIWA), New Zealand.

Cussioli, M. C., Seeger, D., Pratt, D. R., Bryan, K. R., Bischof, K., de Lange, W. P., ... & Pilditch, C. A. (2020). Spectral differences in the underwater light regime caused by sediment types in New Zealand estuaries: implications for seagrass photosynthesis. Geo-Marine Letters, 40(2), 217-225.

Deltares. (2017) User Manual D-Water Quality (Version: 5.06), versatile water quality modelling in 1D, 2D or 3D systems including physical, (bio)chemical and biological processes. Deltares.

Deltares. (2018a). User Manual Delft3D-FLOW (Version: 3.15). Deltares.

Healy, T. and de Lange, W., 2014. Reliability of geomorphic indicators of littoral drift: Examples from the Bay of Plenty, New Zealand. Journal of Coastal Research, 30(2), 301-318. https://doi.org/10.2112/JCOASTRES-D-12-00069.1.

Horstman, E. M., Bryan, K. R., & Mullarney, J. C. (2021). Drag variations, tidal asymmetry and tidal range changes in a mangrove creek system. Earth surface processes and landforms, 46(9), 1828-1846.

La Croix, 2022, Recent and Historical Sedimentation and Sediment Characteristics of Ōhiwa Harbour, New Zealand, Environmental Research Institute Report No. 156. Client report prepared for the Bay of Plenty Regional Council, University of Waikato. 47 pp.

Levy, R., Naish, T., Bell, R., Golledge, N., Clarke, L., Garner, G., ... & Vargo, L. (2020). Te tai pari o Aotearoa–Future sea level rise around New Zealand's dynamic coastline. Coastal Systems and Sea Level Rise: What to Look for in the Future, 4.

Lesser, G. R., Roelvink, J. V., van Kester, J. T. M., & Stelling, G. S. (2004). Development and validation of a three-dimensional morphological model. Coastal engineering, 51(8-9), 883-915.

Lovett, N. J. (2017). Sediment transport in the Firth of Thames mangrove forest, New Zealand (Thesis, Master of Science (MSc)). The University of Waikato, Hamilton, New Zealand. Retrieved from https://hdl.handle.net/10289/11568

MacDonald, I. T. (2009). Flocculation of Fine Sediment in Turbulent Flows. thesis, University of Auckland

Morrison B. 2007. C-management: case studies involving local authorities and Māori, January 2007. Wellington, New Zealand: Local Government New Zealand.

NIWA 2022. CliFlo: NIWA's National Climate Database on the Web.

NZ Government, 2020. National Policy Statement for Freshwater Management 2020, Ministry for the Environment, 70 pp.

Park, S., 2005. Environmental quality of Ohiwa Harbour – 2005, Bay of Plenty Regional Council, Whakatane, New Zealand.

Paul-Burke, K., Ngarimu-Cameron, R., Paul, W., Burke, J., Cameron, K., O'Brien, T., & Bluett, C. (2022). Nga tohu o te taiao: Observing signs of the natural world to identify seastar over-abundance as a detriment to shellfish survival inBoPRCin BoPRC, 2018, State of Environment for Ōhiwa Harbour and Catchment 2018, BoPRC Environmental Publication 2018/8, 99 pp.

Healy, T. and de Lange, W., 2014. Reliability of geomorphic indicators of littoral drift: Examples from the Bay of Plenty, New Zealand. Journal of Coastal Research, 30(2), 301-318. https://doi.org/10.2112/JCOASTRES-D-12-00069.1.

La Croix, 2022, Recent and Historical Sedimentation and Sediment Characteristics of Ōhiwa Harbour, New Zealand, Environmental Research Institute Report No. 156. Client report prepared for the Bay of Plenty Regional Council, University of Waikato. 47 pp.

Richmond, B.M., Nelson, C. S., Healy, T.R., 1984. Sedimentology and evolution of Ohiwa Harbour, Aotearoa/New Zealand. New Zealand Sociology, 37(1), 186-210.

Paul-Burke, K., Burke, J., Te Ūpokorehe Resource Management Team, Bluett, C., & Senior, T. (2018). Using Māori knowledge to assist understandings and management of shellfish populations in Ōhiwa harbour, Aotearoa New Zealand. a barrier-impounded estuarine lagoon in the Bay of Plenty, New Zealand Journal of Marine and Freshwater Research, 52(4), 542-556. 18:461-478.

Rahdarian, A., Bryan, K. R., & Van Der Wegen, M. On the influence of antecedent morphology on development of equilibrium bathymetry in estuaries past and future. Journal of Geophysical Research: Earth Surface, e2022JF006621.

Richmond, B. (1977). Geomorphology and Modern Sediments of Ohiwa Harbour, Bay of Plenty, New Zealand (Doctoral dissertation, University of Waikato).

Richmond, B.M., Nelson, C. S., Healy, T.R., 1984. Sedimentology and evolution of Ōhiwa Harbour, Aotearoa/New Zealand. New Zealand Sociology, 37(1), 186-210.

Robinson, B.J., 2012. Hydrodynamic impacts of tectonics in prehistoric Ohiwa Harbour, North Island, New Zealand, University of Waikato, Hamilton, New Zealand, 111 pp.

Thrush, S. F., Hewitt, J. E., Cummings, V. J., Ellis, J. I., Hatton, C., Lohrer, A., & Norkko, A. J. F. I. E. (2004). Muddy waters: elevating sediment input to coastal and estuarine habitats. Frontiers in Ecology and the Environment, 2(6), 299-306.

Vale, S., Smith, H. Neverman, A., Herzig, A., (2021) Application of SedNetNZ with erosion mitigation and climate change scenarios and temporal disaggregation in the Bay of Plenty Region, Manaaki Whenua – Landcare Research contract to Bay of Plenty Regional Council, Report Number, LC4002.

8. APPENDIX 1

Statistical analyses (bias, accuracy, and skill) were based on Sutherland et al. (2004). Bias was determined following the equation:

$$Bias = \frac{1}{J}\sum_{j=1}^{J}(y_j - x_j) = \langle Y \rangle - \langle X \rangle$$

where Y is the model results, X is the measured data, J is the number of predictions and observations occurring at the same time and location. Angular brackets represent the mean.

Accuracy was determined by the Mean Absolute Error (MAE) and by the root mean square error (RMSE):

$$MAE = \frac{1}{J}\sum_{j=1}^{J}(y_j - x_j) = \langle |Y - X| \rangle$$

$$RMSE = \sqrt{\frac{1}{J}\sum_{j=1}^{J}(y_j - x_j)^2} = \sqrt{\langle (Y-X)^2 \rangle}$$

where straight brackets represent the absolute value of the errors.

Brier skill score was calculated using the following equation:

$$BSS = 1 - \frac{MSE(Y,X)}{MSE(B,X)} = 1 - \frac{\langle (Y-X)^2 \rangle}{\langle (B-X)^2 \rangle}$$

where B is the average of measured data.

The classification based on BSS score ranges from bad to excellent according to Sutherland et al. (2004):

BSS score	**Classification**
BSS <0.0	bad
0.0> BSS <0.1	poor
0.1> BSS <0.2	reasonable/fair
0.2> BSS <0.5	good
0.5> BSS <1.0	excellent

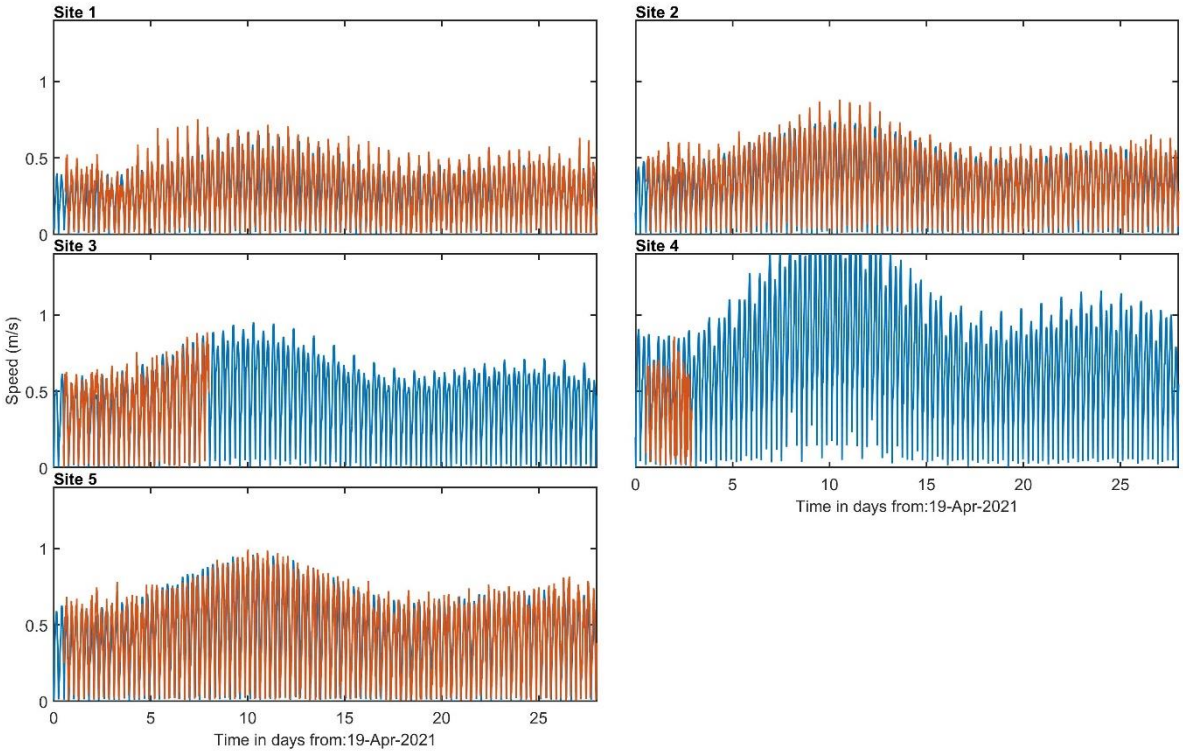

Figure A1: *Observed speed (red) and modelled speed (blue) at the sites shown in Figure 1: Field site including deployment locations and the location of stream inflows (background image is from Sentinel-2 satellite data).*

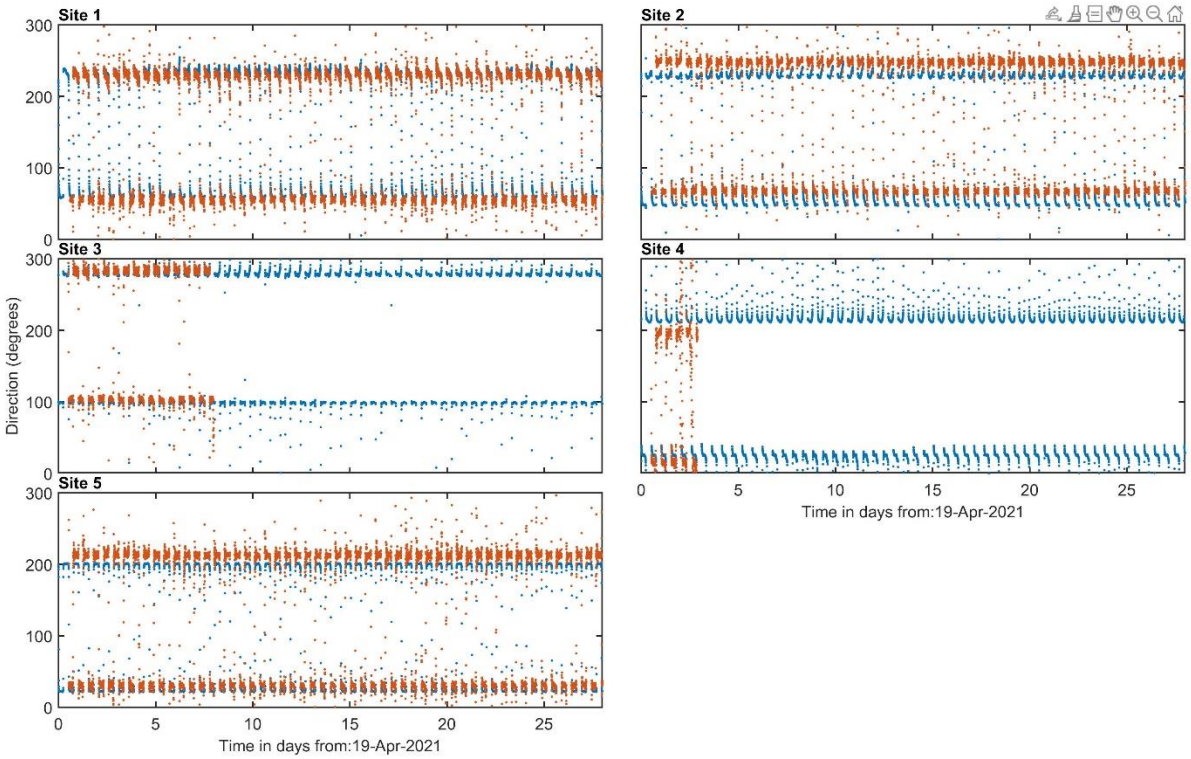

Figure A2: *Observed direction (red) and modelled direction (blue) at the sites shown in Figure 1: Field site including deployment locations and the location of stream inflows (background image is from Sentinel-2 satellite data).*

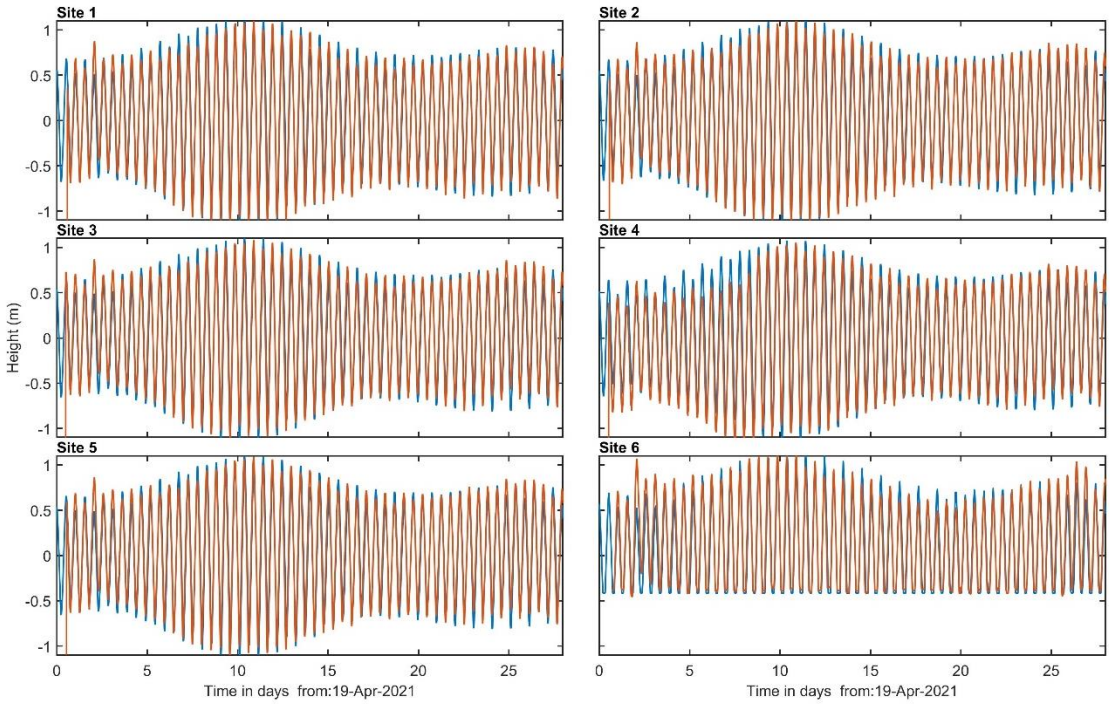

Figure A3: *Observed waterlevel (red) and modelled waterlevel (blue) at the sites shown in Figure 1: Field site including deployment locations and the location of stream inflows (background image is from Sentinel-2 satellite data).*

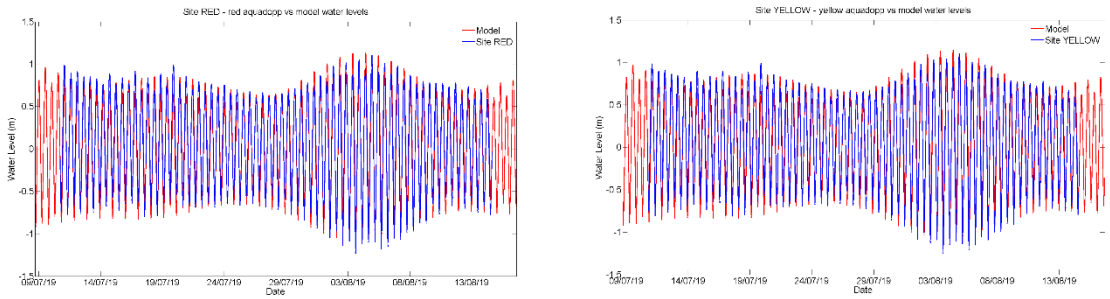

	BIAS	MAE	RMSE	BSS
'site RED - Megan	-0.029	0.137	0.165	0.902
'site YELLOW - Megan'	-0.021	0.138	0.169	0.897

Figure A4: *Observed waterlevel (red) and modelled waterlevel (blue) for Megan Raiapa's deployment undertaken during her MSc in 2019.*

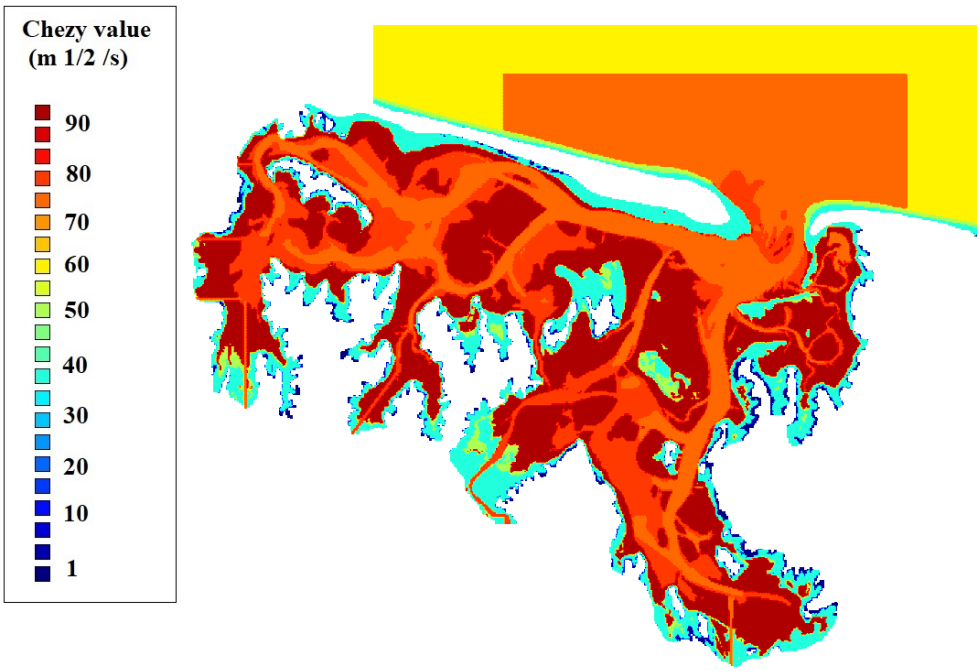

Figure A5: *Spatially varying bottom roughness map (Chézy) used for model calibration.*

9. APPENDIX 2

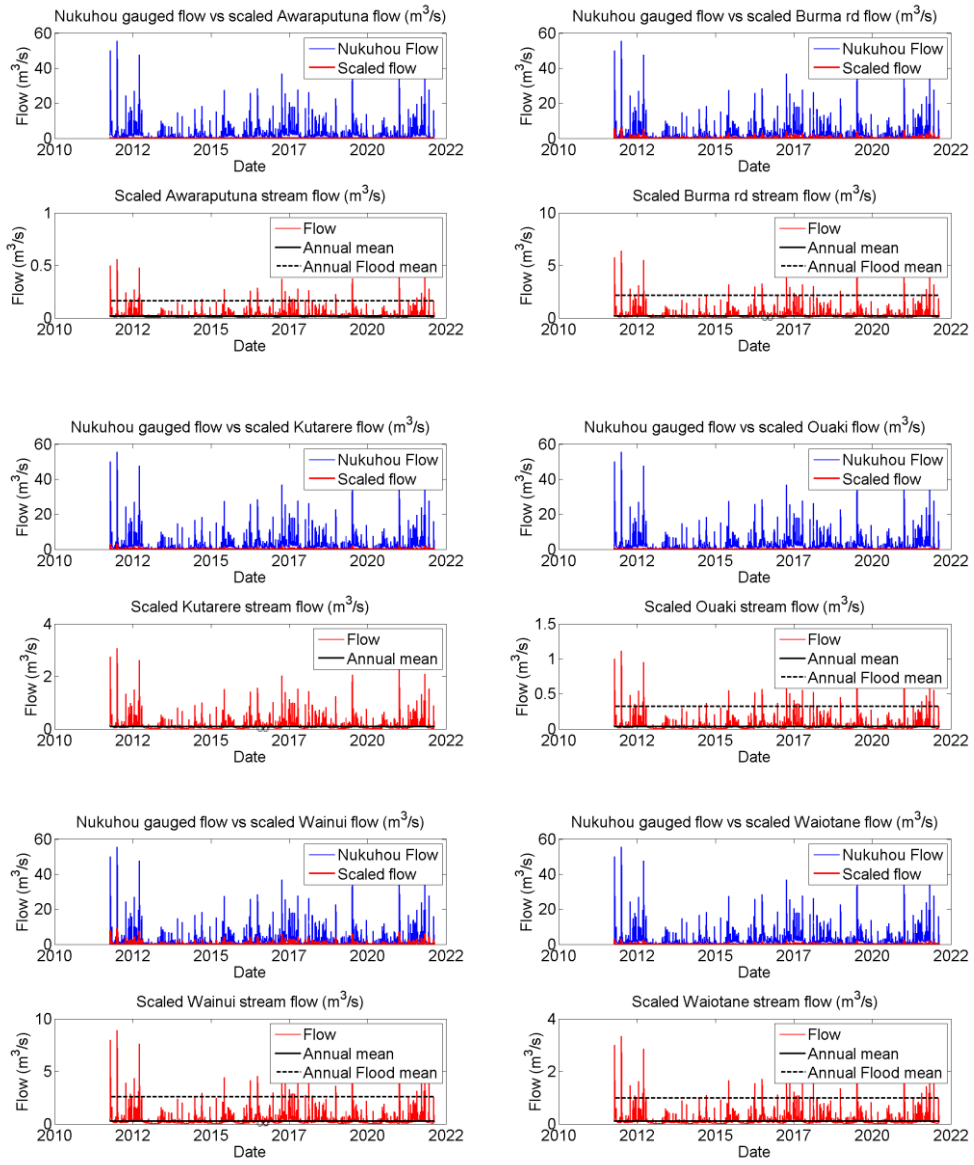

Figure A6: *Recreated stream discharge time series for ungauged catchments*

10. APPENDIX 3

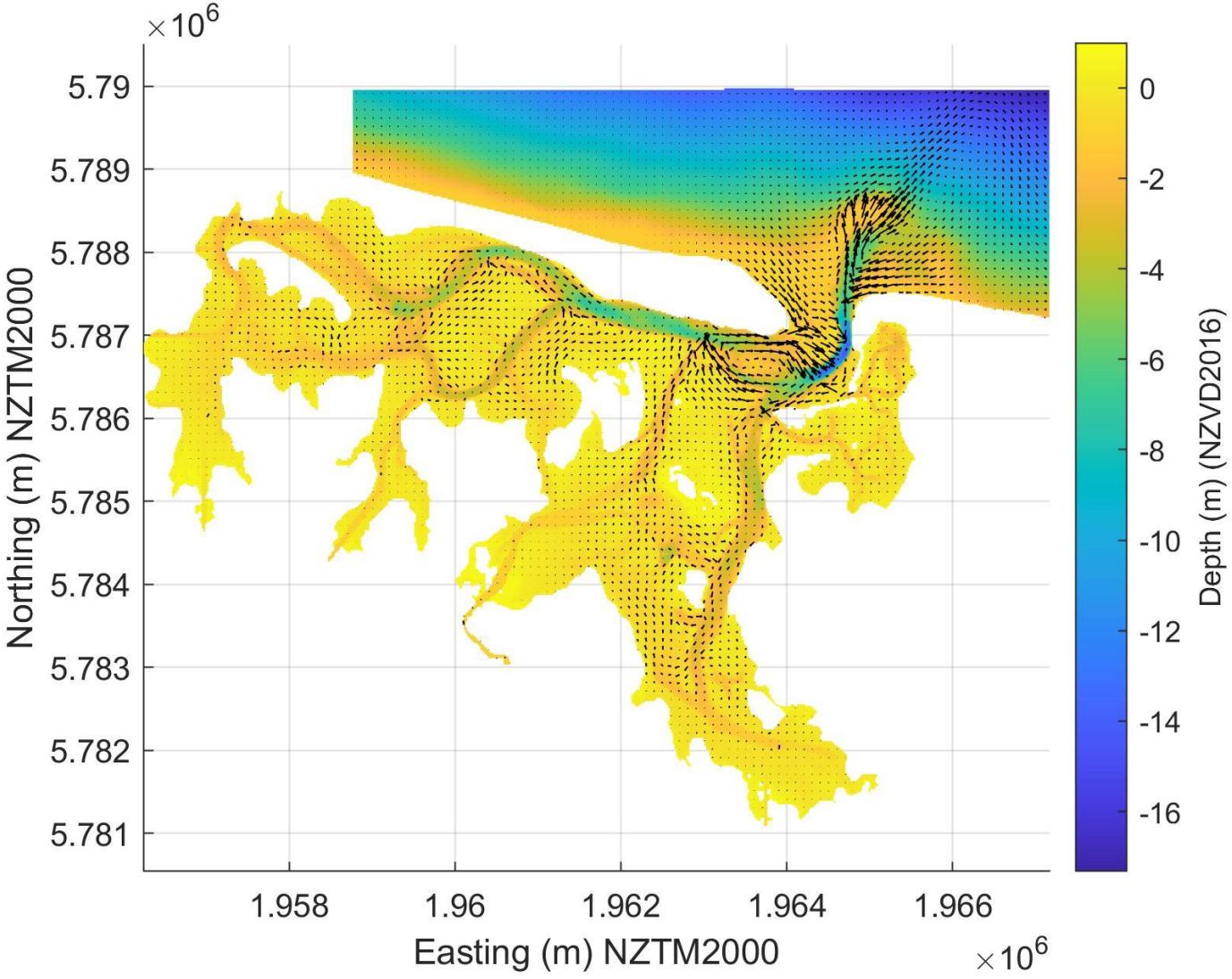

Figure A7: *High resolution version of tidal residual currents.*

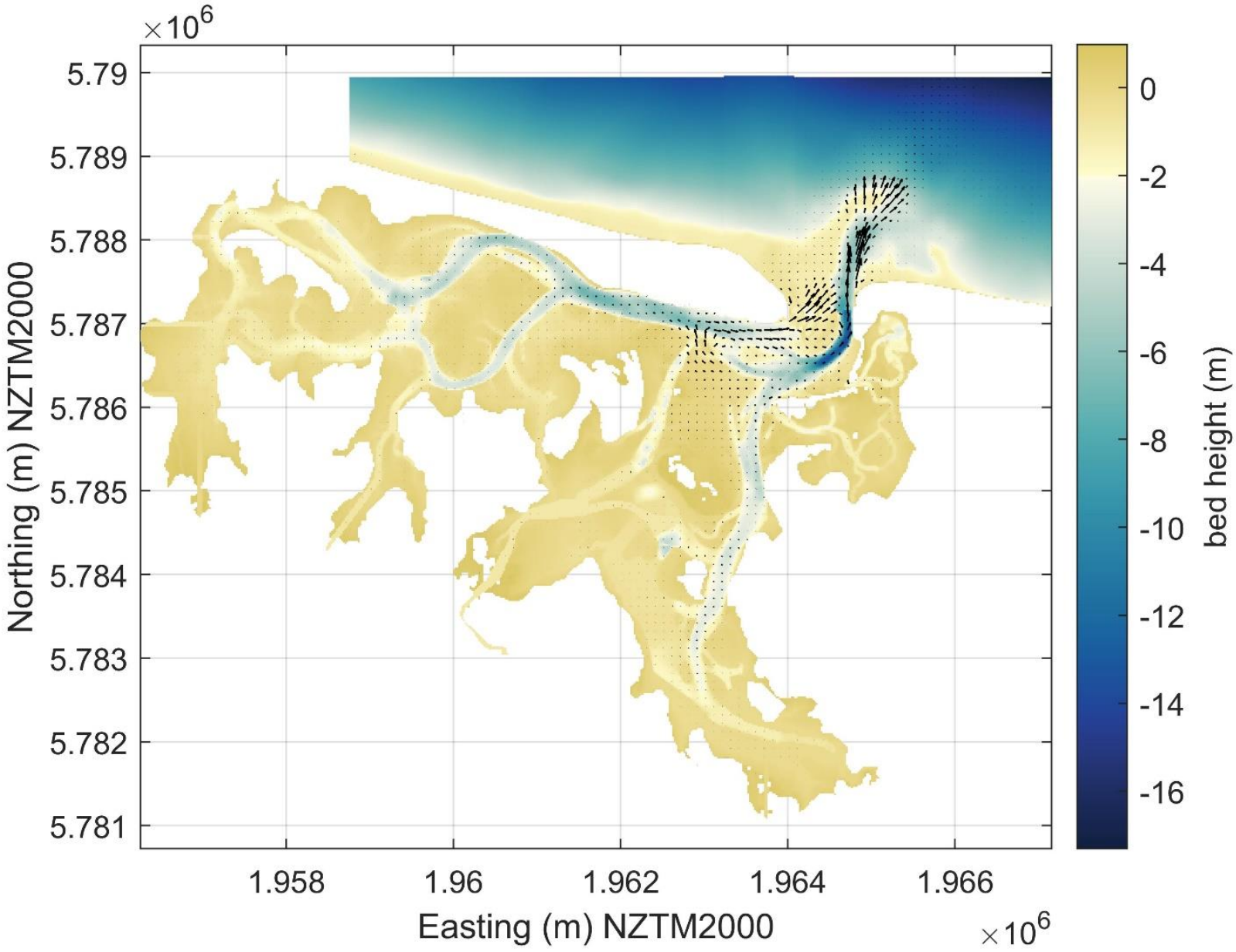

Figure A8 *High resolution version of residual sediment fluxes.*

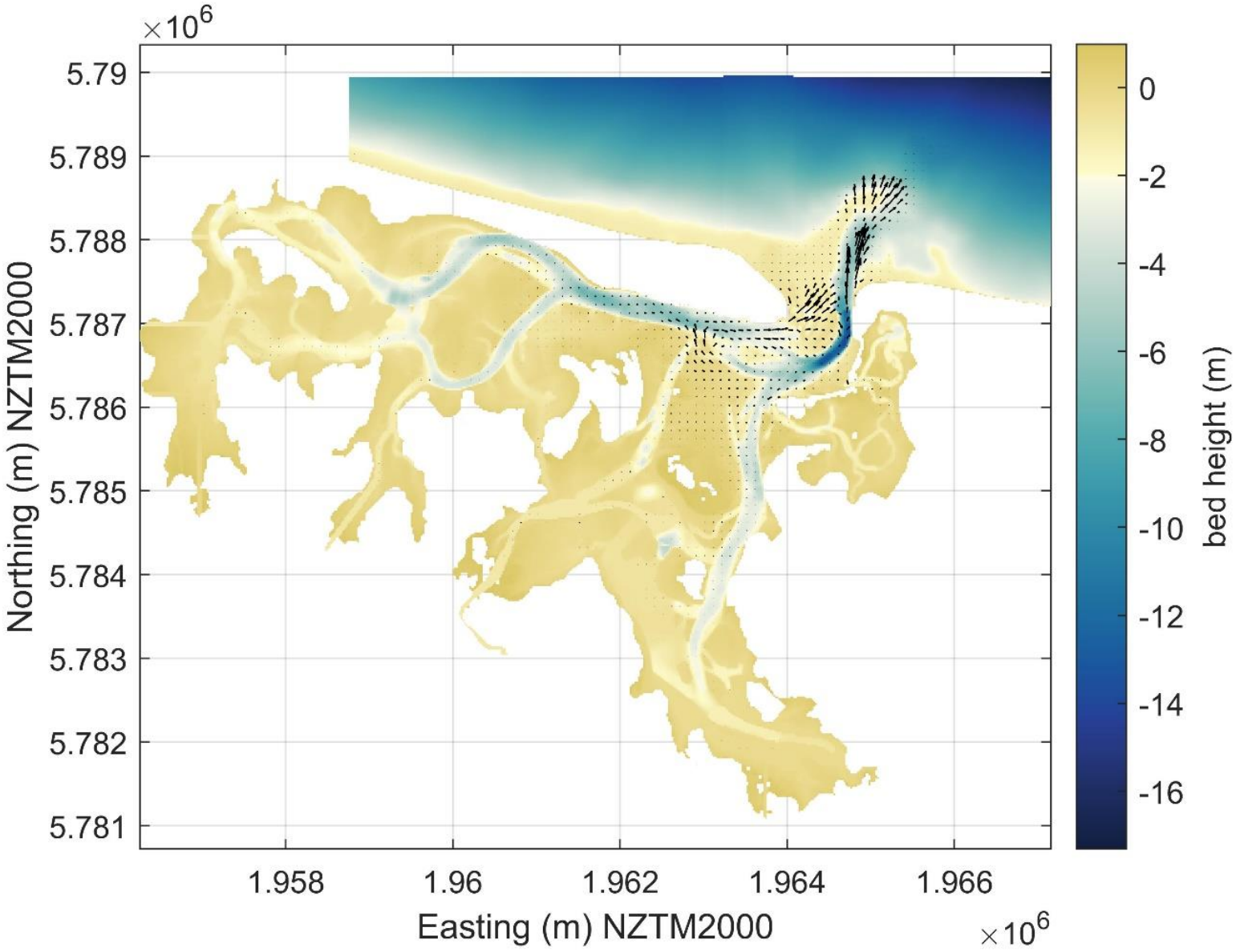

Figure A9 *High resolution version of residuals and fluxes.*

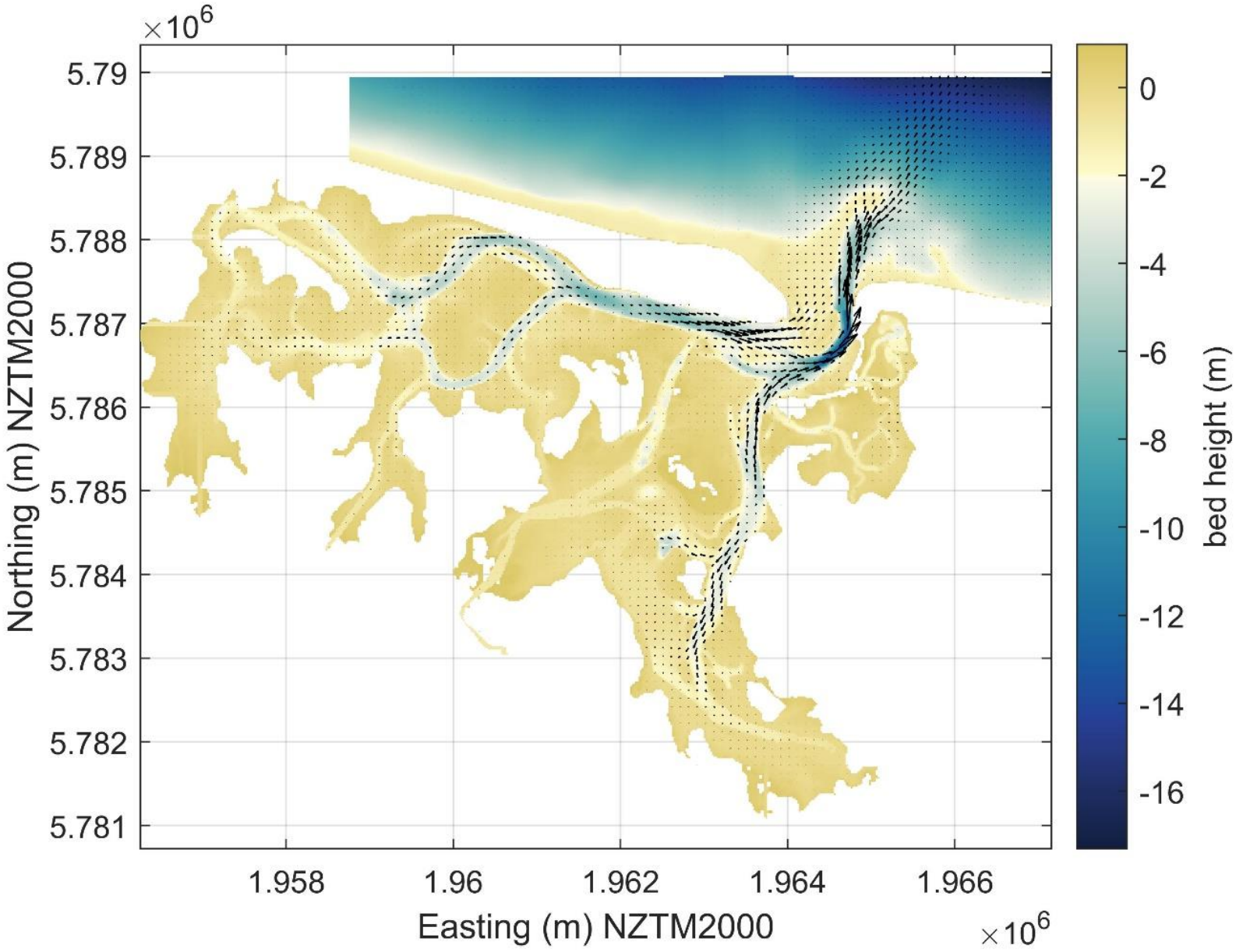

Figure A10 *High resolution version of residual mud fluxes.*

11. APPENDIX 4

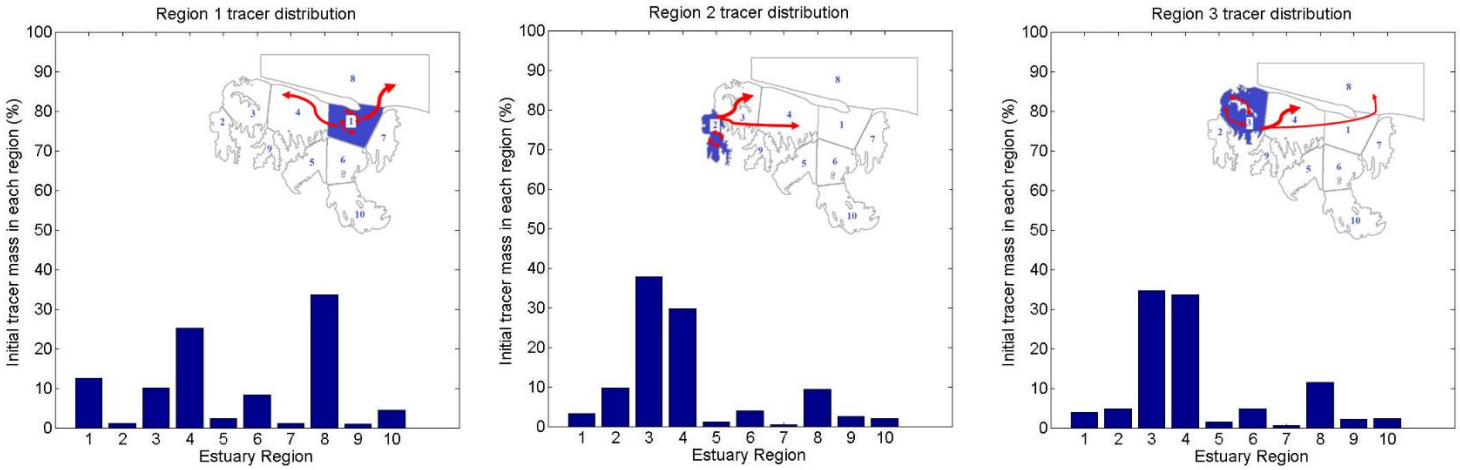

Figure A11: *Results of tracer releases from individual harbour regions. Red arrows indicate the top 3 regions where tracer spends in another region of the harbour (over the simulation period of 1 month). Tracer mass initially released in region 1 (left panel) is mostly advected offshore to region 8 as well as to region 4. Tracer mass initially released from region 2 (middle panel) is mostly advected to region 3 and 4, with little exchange to regions 5 and 6. Tracer mass initially released from region 3 (right panel) remains in region 3 or is advected to region 4, with little exchange with regions 5 and 7.*

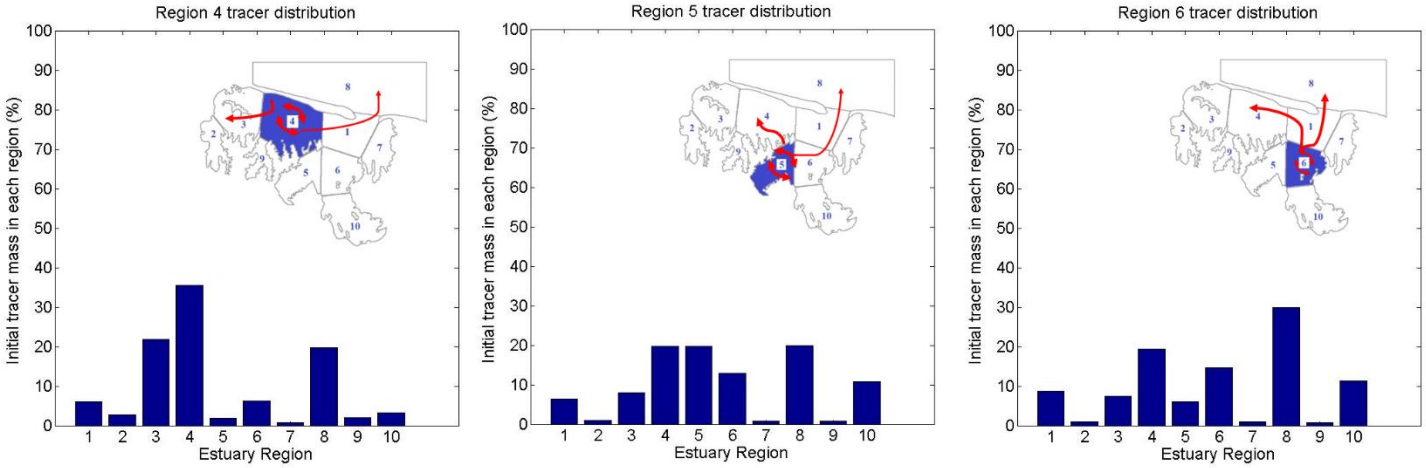

Figure A12: *Results of tracer releases from individual harbour regions. Red arrows indicate the top 3 regions where tracer spends in another region of the harbour (over the simulation period of 1 month). Tracer mass initially released in region 4 (left panel) mostly remains in region 4 or is advected offshore to region 8 as well as to region 3. Tracer mass initially released from region 5 (middle panel) is mostly trapped or advected to region 8, 4, and 10 with little exchange to regions 2 and 7 and 9. Tracer mass initially released from region 6 (right panel) is advected offshore to region 8 and to region 4, with little exchange with regions 2, 7 and 9.*

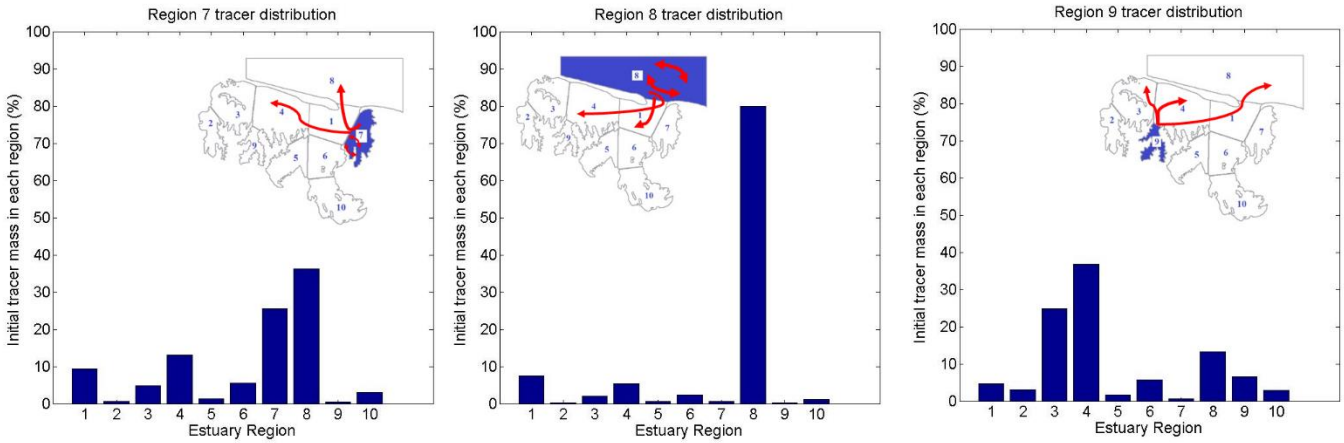

Figure A13: *Results of tracer releases from individual harbour regions. Red arrows indicate the top 3 regions where tracer spends in another region of the harbour (over the simulation period of 1 month). Tracer mass initially released in region 7 (left panel) is mostly advected offshore to region 8, is recirculated within its region or moves to region 4 and 1. Tracer mass initially released from region 8 (middle panel) is mostly mixed offshore in region 8, with regions 1 and 4 receiving most of the mass and regions 2 and 9 exchanging the least with the ocean. Tracer mass initially released from region 9 (right panel) is advected to region 4 and 3, with little exchange with regions 5 and 7.*

12. APPENDIX 5

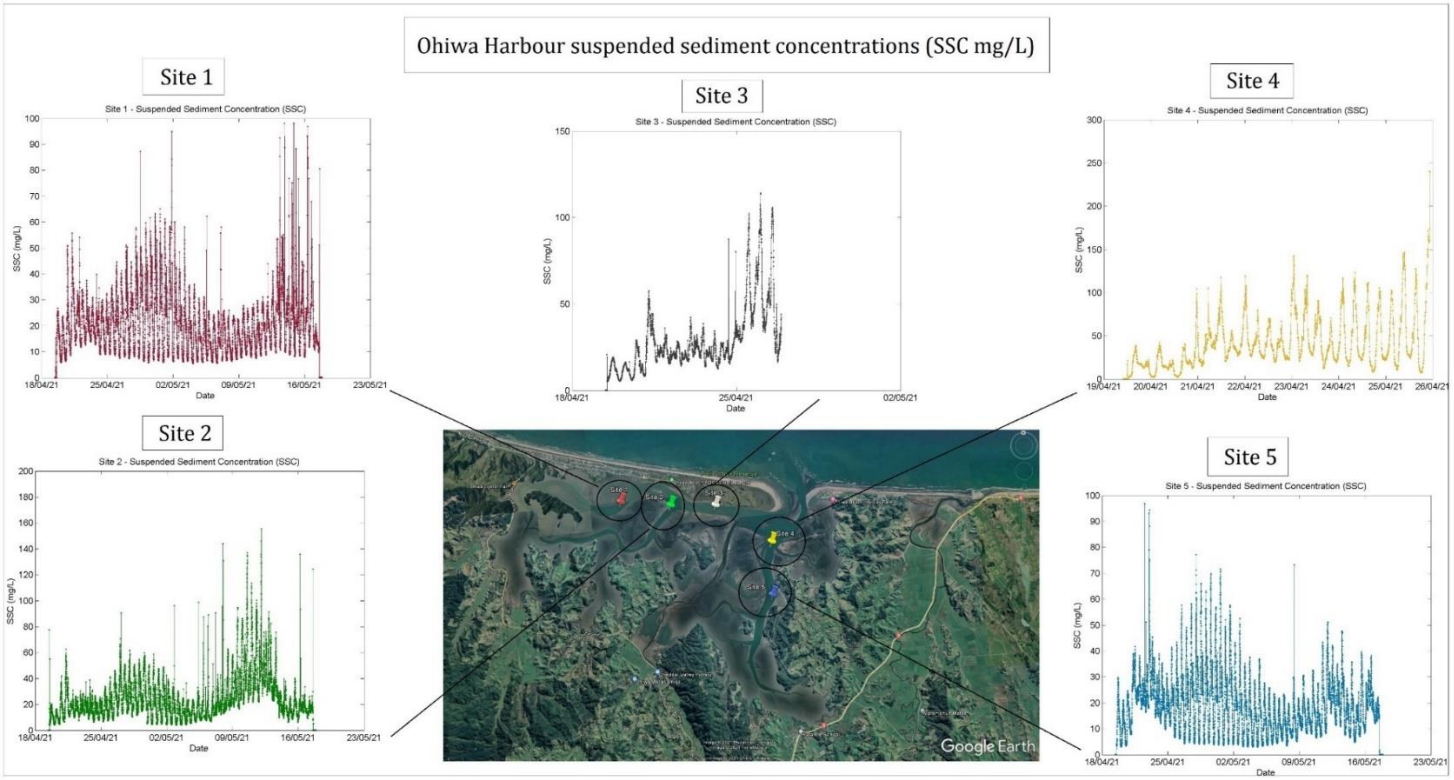

Figure A14: *Field measurements of suspended sediment concentrations (mg/L) from each instrument location within Ōhiwa Harbour over the calibration period (19/4/21 – 17/5/21). Optical backscatter sensors (OBS3+) deployed with 'Nortek Aquadopps' instruments were calibrated in the lab with native sediments post deployment to convert instrument voltage/counts to suspended sediment concentrations (mg/L). Instruments at sites 3 and 4 were buried with sediment during the calibration period.*

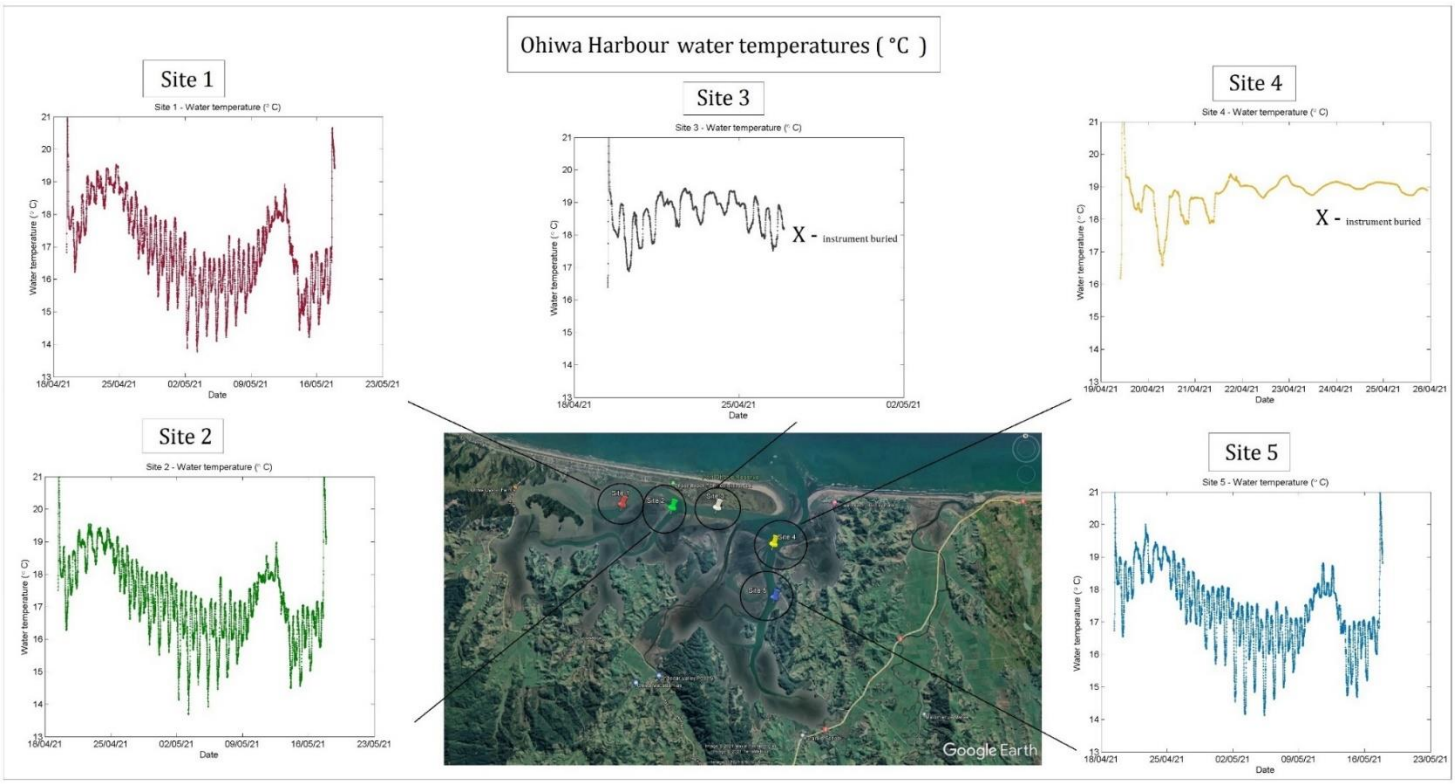

Figure A15: *Field measurements of water temperature (degrees Celsius) from each of the 'Nortek Aquadopp' instrument location within Ōhiwa Harbour over the calibration period (19/4/21 – 17/5/21). Variations in water temperature observed over the measured period coincide with weather events and rainfall. Instruments at sites 3 and 4 were buried with sediment during the calibration period.*

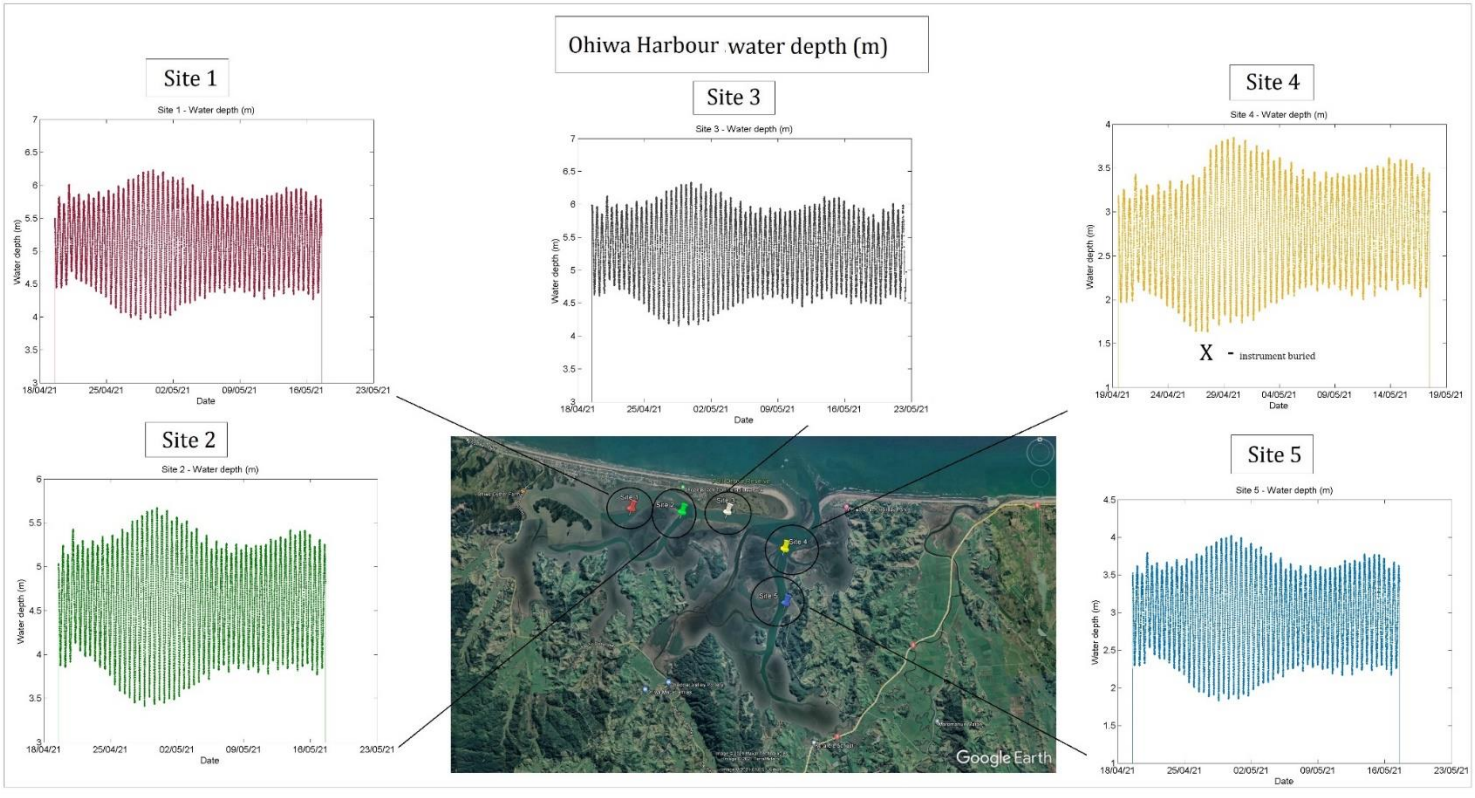

Figure A16: *Field measurements of water depth (metres) converted from pressure below water surface from each of the 'Nortek Aquadopp' instrument location within Ōhiwa Harbour over the calibration period (19/4/21 – 17/5/21). The spring-neap tidal pattern and magnitude is reflected in the water depth variations. Instruments at sites 3 and 4 were buried with sediment during the first week of calibration period but still contain pressure (depth) data over the entire period.*